Sediment cover modulates landscape erosion patterns and channel steepness in layered rocks: insights from the SPACE Model

G. J. Guryan[1], J. P. Johnson[1], and N. M. Gasparini[2]

[1]Department of Earth and Planetary Sciences, Jackson School of Geosciences, University of Texas at Austin, Austin, TX, USA

[2]Department of Earth and Environmental Sciences, School of Science and Engineering, Tulane University, New Orleans, LA, USA.

Corresponding author: Grace Guryan (gguryan@utexas.edu)

Key Points:

- We use a numerical landscape evolution model to explore how sediment cover affects channel evolution in layered rocks
- Sediment cover dampens the erosional feedbacks that arise in layered rocks when weak rock undercuts harder rock
- Sediment reduces the effective erodibility contrast between rock types, increasing steepness in weak rocks and reducing it in harder ones.

Abstract

Erosional perturbations from changes in climate or tectonics are recorded in the profiles of bedrock rivers, but these signals can be challenging to unravel in settings with non-uniform lithology. In horizontally layered rocks, the surface lithology at a given location varies through time as different layers of rock are exposed. Recent modeling studies have used the Stream Power Model (SPM) to highlight complex variations in erosion rates that arise in bedrock rivers incising through layered rocks. However, these studies do not capture the effects of coarse sediment load on channel evolution. We use the "Stream Power with Alluvium Conservation and Entrainment" (SPACE) model to explore how sediment cover influences landscape evolution and modulates the topographic expression of erodibility contrasts in horizontally layered rocks. We simulate river evolution through alternating layers of hard and soft rock over million-year timescales, with a constant uplift rate of 1 mm/year. Compared to the SPM, model runs with sediment cover have systematically higher channel steepness values in soft rock layers and lower channel steepness values in hard rock layers. As sediment cover effects increase, the contrast in steepness between the two rock types decreases. Effective bedrock erodibilities back-calculated assuming the SPM are strongly influenced by sediment cover. We also find that sediment cover can significantly increase total relief and timescales of adjustment towards landscape-averaged steady-state topography and erosion rates.

Plain Language Summary

Bedrock river profiles are commonly used to make interpretations about tectonics, climate, and lithology, but isolating these signals is challenging in settings with non-uniform lithology. In horizontally layered rocks in particular, lithologic variations result in complex patterns in channel slope and erosion rates through space and time. Lithology is also important for channel evolution because it influences the amount and characteristics of the sediment that's eroded from the channel bed. In turn, sediment can inhibit erosion by being deposited and armoring the channel bed. In our study, we use a landscape evolution model that explicitly captures the production and deposition of sediment to test how sediment cover influences channel steepness and erosion rates in horizontally layered rocks. We find that sediment cover can significantly dampen the variations in erosion rate that have been observed in other modeling studies of layered rocks. Sediment cover also results in steeper channel slopes in soft rock layers and reduces steepness in hard rocks. These findings are important because many analyses of river profiles don't explicitly consider the role of sediment, but our results show that sediment can have a dramatic influence on how lithologic contrasts are expressed in channel profiles.

1. Introduction

Climatic and tectonic signals are recorded in the profiles of bedrock river channels, which can be used to make inferences about these signals as they propagate through landscapes (Crosby

& Whipple, 2006; Kirby & Whipple, 2012; Norton & Schlunegger, 2011; Whittaker, 2012; Wobus et al., 2006). However, distinguishing between climatic and tectonic effects on river channel evolution is hampered by our relatively limited understanding of lithology's influence on channel steepness and erosion rates (Chilton & Spotila, 2022; Gasparini & Whipple, 2014; Kirby & Whipple, 2012; Shobe et al., 2020). Lithology controls channel evolution in two main ways: by setting the erodibility of the channel substrate and by producing coarse sediment. Bedrock erodibility is a model-dependent parameter that represents how efficiently rock will erode under a given hydraulic forcing. It encompasses a combination of rock strength, the degree of fracturing, weathering, and climate (Whipple & Tucker, 1999). Lithology also influences the size and quantity of sediment delivered to channels as a result of differences in both fracture spacing, strength, and susceptibility to weathering (Anderson et al., 2023; Neely & DiBiase, 2020; Scott & Wohl, 2019; Sklar et al., 2017). Coarse sediment can aid or inhibit channel incision, by acting as both tools that abrade the bed and by armoring it from grain impacts and other erosion processes (referred to as the *cover effect*) (Sklar & Dietrich, 2004). Several studies have shown that channels within the same lithology that are mantled with coarse sediment tend to be steeper (DiBiase et al., 2018; Johnson et al., 2009; Shobe et al., 2020; Sklar et al., 2017; Thaler & Covington, 2016).

Recent modeling studies have shown that the stratigraphic order of soft vs. hard rocks influences landscape evolution by controlling local erosion rate history. In layered rocks different units are exposed at the surface at different times, causing both spatial and temporal variations in erosion rates (Darling et al., 2020; Forte et al., 2016; Perne et al., 2017; Wolpert & Forte, 2021; Yanites et al., 2017). Forte et al. (2016) and Perne et al., (2017) assumed threefold bedrock erodibility contrasts between weak and strong units to simulate plausible stream channel profiles. Yanites et al. (2017) found that a twofold difference in erodibility between modeled rock units (limestone and shale in their study) was required to produce a model output comparable to modern topography of the Eastern Jura Mountains, Switzerland. In contrast, other work has suggested that bedrock erodibility should scale inversely and nonlinearly with rock tensile strength (Müller-Hagmann et al., 2020; Sklar & Dietrich, 2001), predicting much larger much larger erodibility contrasts between different rock types than have been inferred in field settings from topography and erosion rates. The disconnect between mechanistically predicted erodibilities and those measured empirically is not well understood.

Most landscape evolution modeling studies exploring lithology-dependent erodibility contrasts have used the Stream Power Model (SPM), which assumes that local erosion rate scales with local slope and drainage area (e.g. Darling et al., 2020; Forte et al., 2016, Perne et al., 2017, Yanites et al., 2017). This simple and flexible model has provided a quantitative framework for interpreting signals of tectonic and climatic forcing from real landscapes (e.g., Harel et al., 2016, Pavano et al., 2016, Roberts and White, 2010; Whipple and Tucker, 1999; Whittaker et al., 2008; Wobus et al., 2006). Nonetheless, the SPM assumes that channel erosion rates are "limited" by the ability of the flow to detach bedrock, and that the sediment load does not also control incision (or that its effects can be fully accounted for through a lumped erodibility coefficient). The influence of sediment cover inhibiting channel incision could partially explain the different ranges of erodibility contrasts that have been predicted by models or observed in field and laboratory settings. We use the term effective erodibility to describe the apparent erodibility of a given channel reach that results from channels adjusting their slopes due to sediment cover.

Here we test how sediment cover affects the topographic expression of lithologic contrasts in layered rocks using the Stream Power with Alluvium Conservation and Entrainment (SPACE) model (Shobe et al., 2017). The SPACE model expands on the SPM to incorporate both the production of sediment from erosion of the upstream watershed, and conservation of mass as sediment is transported or deposited downstream. The model accounts for the cover effect (sediment load inhibiting bedrock incision) but not the tools effect, instead following the SPM in assuming that erosion rate is proportional to stream power. We hypothesize that sediment cover systematically increases steepness in soft rocks, lessening the effective erodibility contrast between hard and soft layers. We also explore how varying degrees of sediment cover influence adjustment timescales of numerical landscapes.

2. Models and Methods

2.1 The Stream Power Model

The SPM is arguably the most commonly used framework for analyzing the topography of river profiles as well as for modeling fluvial incision (Howard, 1994; Whipple & Tucker, 1999). The stream power model assumes that the erosion rate is a power-law function of stream power (or bed shear stress) and predicts fluvial incision as a function of the upstream drainage area (A), erodibility (K), topographic slope (S) and scaling exponents m and n (Howard & Kerby, 1983; Lague, 2014; Whipple & Tucker, 1999):

$$E = K\,A^m\,S^n \quad (1)$$

The dimensions of *K* depend on exponent m as $L^{1-2m}T^{-1}$, where L and T are length and time respectively (Whipple and Tucker, 1999). While a value for *K* is usually assumed in modeling studies, for field-based applications it can empirically be back-calculated from equation (1) (e.g., $K = EA^{-m}S^{-n}$) based on erosion rates (e.g. from cosmogenic radionuclides, terraces, or other methods) and DEM measurements (*A, S*) or other topographic constraints (Barnhart et al., 2020; Wobus et al., 2006) It is important to note that *K* is a lumped parameter that theoretically accounts for not only local bedrock properties but is also a nonlinear function of erosion process, sediment load, hydraulic geometry, and basin hydrology (Whipple and Tucker, 1999).

The scaling exponents *m* and *n* are also key parameters in the stream power model. The most commonly used values for the scaling exponents in the SPM are probably *n=1* and *m=0.5* (Ferrier et al., 2013; Lague, 2014; Murphy et al., 2016). However, Lague (2014) argues for *n*>1 based on erosion thresholds and hydrologic variability. Based on a global compilation of erosion rates and topography, Harel et al. (2016) also suggest *n*>1. Perne et al. (2017) found that in layered rocks, instead of achieving true topographic steady state, channels adjust to a continuity steady state where the rate of retreat in the direction *parallel to contacts* is equal in layers of different erodibility. Geometrically, this means that erosion rates--measured vertically, as erosion is usually defined--will not be equal in layers with different erodibilities unless the contacts between layers are also vertical. Furthermore, Perne et al. (2017) found that when *n*=1 in horizontal or subhorizontal layers, the channel is no longer able to maintain continuity by adjusting its slope. When *n* <1, weak rock erodes faster (measured vertically) and steeper channel segments are found in weaker rocks. When *n*>1, channel segments with strong rock erode faster (measured vertically) and are steeper. Given these findings, we use *m*=0.75 and *n*=1.5 for all of our simulations, allowing the channel to adjust its slope and maintaining an *m/n* ratio of 0.5. This gives K in units of $m^{-0.5}yr^{-1}$ (where m is meters, not the exponent).

2.2 The SPACE Model

The SPACE model builds on the SPM by adding terms for conservation and transport of eroded mass (i.e., sediment) (Shobe et al., 2017). Within the channel network, the SPACE model allows for sediment to be eroded from the bed and entrained from an alluvial layer, transported downstream, and deposited. The SPACE model can transition smoothly between detachment-

limited (i.e., SPM), mixed-bedrock alluvial, and fully transport-limited behaviors. Bedrock erosion rate E_r is modeled as

$$E_r = (K_r q S^n - \omega_{cr}) e^{-H/H_*} \quad (2)$$

where K_r is bedrock erodibility, q is water discharge per unit channel width, ω_{cr} is a stream power bedrock erosion threshold, H is the average thickness of sediment covering the bed, and H_* is a bedrock roughness length scale measured vertically. Table 1 presents parameter values used in most model runs. We further separate K_r into K_{soft} and K_{hard}, representing the weaker and stronger lithological units, respectively. Following Shobe et al. (2017), all of our model runs assume $\omega_{cr} = 0$ for simplicity and to reduce the number of unconstrained variables in the analysis. The "cover effect" of bed alluviation inhibiting incision is expressed by e^{-H/H_*}; in particular it represents the relative exposure of bedrock, which decreases following exponential decay as average alluvial thickness increases and the rough bedrock surface becomes increasingly buried (Hancock & Anderson, 2002; Turowski et al., 2007). Bedrock erosion becomes negligible ($e^{-H/H_*} \approx 0$) when H/H* approaches a value of ≈6. In our study, H* is set to 1.0 m.

The rate of entrainment of sediment from the bed (E_s) is calculated as:

$$E_s = (K_{sed} q S^n - \omega_{cs})\left(1 - e^{-H/H_*}\right) \quad (3)$$

Where K_{sed} is sediment erodibility and ω_{cs} is a stream power sediment erosion threshold. Again following Shobe et al. (2017), all of our model runs assume $\omega_{cs} = 0$ for simplicity. The $1 - e^{-H/H_*}$ term dictates that sediment entrainment rate decreases as the average thickness of bed alluvium decreases and more bedrock area is exposed. The thickness of the alluvial layer (H) evolves over time due to E_s and the rate of sediment deposition on the the bed (D_s):

$$(1 - \phi)\frac{\partial H}{\partial t} = D_s - E_s = \frac{q_s}{q} V - E_s \quad (4)$$

Where ϕ is sediment porosity, q_s is sediment flux per unit width, and V is an effective grain settling velocity which largely controls D_s. With $\omega_{cs} = 0$, two different parameters in the SPACE model control the behavior of sediment: V and K_s. Following Shobe et al. (2017), discharge is implemented as $q = k_q A^m$, and coefficient k_q is subsumed into K_r and K_{sed} rather than treated independently. Therefore when $V = 0$ (sediment never settles to the bed) then $H = 0$ and equation (2) is equivalent to the standard SPM (equation 1). A complete list of SPACE

model parameters is presented in Table 1; readers are referred to Shobe et al. (2017) for additional SPACE model equations and parameter descriptions.

2.3 Channel Steepness Index

Normalized channel steepness index (k_{sn}) is a topographic metric useful for interpreting channel slope differences across drainage areas (e.g., Flint, 1974; Whipple and Tucker, 1999):

$$k_{sn} = \frac{S}{A^{-\theta_{ref}}} \quad (5)$$

Where θ_{ref} is a "reference" channel concavity, typically the average concavity across a region of interest. In natural landscapes, concavity indices typically ranges from approximately 0.4-0.6 (Kirby & Whipple, 2012). When calculated based on the SPM (equation 1), assuming the landscape is eroding at steady state such that $E = U$ (where U is rock uplift rate) and assuming $\theta_{ref} = m/n$ yields

$$k_{sn} = \left(\frac{U}{K}\right)^{1/n} \quad (6)$$

This steady-state SPM relation has widely been used for interpreting signals of tectonic and climatic forcing from longitudinal channel profiles as it simply relates topography to uplift rate as well as to erodibility (e.g., DiBiase et al., 2010, Kirby and Whipple, 2001, Wobus et al., 2006). The m/n value of 0.5 used in our model runs gives k_{sn} in units of meters.

.The equation for normalized steepness index using the SPACE model at steady state ($E = U$) follows the same general form as the SPM, with an added term to account for the alluvial layer:

$$k_{sn} = \left[U\left(\frac{V}{rK_{sed}} + \frac{1}{K_r}\right)\right]^{1/n} \quad (7)$$

where r is a runoff rate. Ignoring spatial and temporal variability in the amount of precipitation that runs off of hillslopes (i.e. uniform precipitation with no infiltration or evapotranspiration), r is simply equal to the precipitation rate. For $V = 0$ equation (7) matches (6).

2.4 Model Configuration

We implement the SPACE model using the Landlab Toolkit, an open-source python-based modeling library (Hobley et al., 2017) designed for modeling earth surface processes. We couple the SPACE Large Scale Eroder component with Landlab's LithoLayers component (Barnhart et al., 2018) to simulate channel incision through alternating layers of hard and soft rock at million-year timescales. All models are run on a square grid with closed boundaries and a single outlet at the lower left corner of the grid. Models are run for either 0.8 or 1.2 million years with a constant and uniform rock uplift rate of 1.0 mm/yr. Over 1.2 myr, uplift cycles through the stack of 10 layers illustrated in Figure 1 three times. For simplicity, our models do not incorporate any hillslope processes and focus solely on channels. We first present an SPM and a SPACE model run on 200x200 cell grids that run for 800 kyr (Table 1), then present a series of runs on smaller 50x50 cell grids focused on exploring the model parameter space that run for 1.2 myr (Table 2). For each model run, we calculate the expected steady state channel steepness for each rock layer using equations 6 (for SPM runs) and 7 (for SPACE model runs). We then compare these expected values against our model output to explore how the interaction between hard and soft layers influences channel steepness. We also explore how differences in sediment transport efficiency and corresponding thicknesses of sediment cover influence channel evolution by systematically varying three main model parameters: the "effective" settling velocity of the sediment (V), the erodibility of the alluvial layer on the bed (K_{sed}), and the ratio of the erodibilities of the hard and soft bedrock layers (Table 1, 2). For both 200x200 cell model runs, the erodibility of the soft rock is held constant at K_{soft}=1.0x10^{-5} ($m^{-0.5}yr^{-1}$) while the erodibility of the hard rock is set to one fifth of the erodibility of the soft rock (K_{hard} = 2x10^{-6} $m^{-0.5}yr^{-1}$).

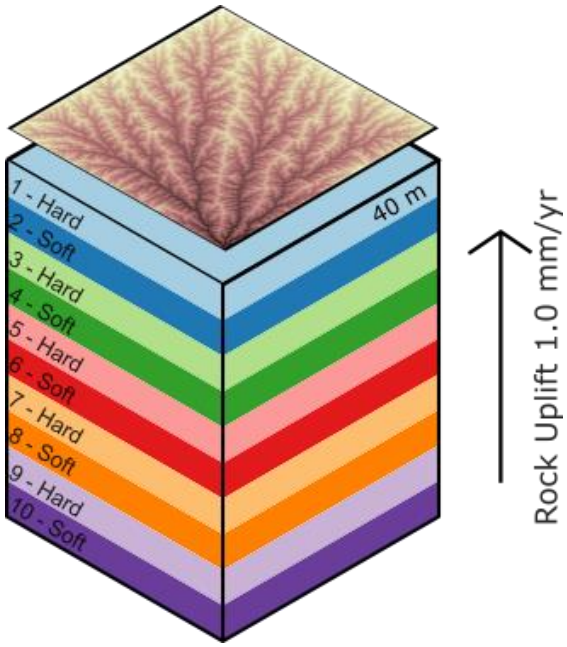

Figure 1. Layer configuration and initial drainage network. The initial drainage network has sub-meter scale relief. Layers alternate between hard and soft rock, and each layer is numbered from 1-10 to clearly distinguish between layers along the channel profile. Layers 1-10 are repeated for the duration of the model run so that the model can continually erode alternating layers of hard and soft rock.

Each grid uses the same initial drainage network so that channel profiles can be compared across model runs. Following the approach of Shobe et al. (2017) we created an initial drainage network by imposing an initial random roughness on the topographic surface then computing fluvial erosion using an SPM model run for 500 kyr to establish a steady state drainage network. We then scale the topographic elevations of the previously-created steady state drainage network down by a factor of .01 to produce a sub-meter scale topography with an established drainage network as the initial condition for the SPACE model runs (Figure 1).

Arguably, a significant limitation of the SPACE model equations is that grain diameter is not an explicit model parameter; this makes quantitative comparison to field sites more difficult. Nonetheless, varying V and K_{sed} across different model runs allows us to compare the relative influence of coarser (higher V, lower K_{sed}) vs. finer sediment (lower V, higher K_{sed}). Particle settling velocity reflects a combination of particle size, flow conditions, and the concentration of sediment in the water column (Davy & Lague, 2009). However, as formulated in the SPACE model, "effective" settling velocity V cannot be mapped directly to a meaningful grain size because V is a lumped parameter that, in this model, is implicitly biased by flow intermittency and hydrograph variability. Timescales of actual physical grain settling in streams are orders of magnitude larger than model timesteps (40 and 100 years in our runs; Table 1 and 2, respectively). For example, Shobe et al. (2017) impose V between 1 and 5 m/yr, far slower than physical for coarse sediment (gravel to boulders) that is relevant for cover effects. Nonetheless, in the model, faster settling velocities represent larger grains while slower settling velocities represent finer grains. Matching the range of values explored by Shobe et al. (2017), for this study we test particle settling velocities of 1.0, 3.0, and 5.0 m/yr. We also compare these model runs against an SPM model, where particle settling velocity is effectively zero. Sediment particle size is also conceptually reflected in the erodibility of the alluvial layer (K_{sed}). Smaller grains require less shear stress to be lifted off the bed and entrained in the flow, so an alluvial layer composed of uncohesive fine sediment will be more erodible than one made up of coarse sediment. Both V and K_{sed} affect the total degree of sediment cover in the model. In the SPACE model the dimensionless sediment entrainment ratio $K_{sed}q/V$ reflects the competition between sediment entrainment (controlled by $K_{sed}$and discharge, q) and deposition (controlled by V) (Shobe et al., 2017) (Table 2).

We also explore how varying degrees of sediment cover influence what we refer to as the "effective erodibility" of a given channel reach. In the present modeling study, we impose values for bedrock erodibility *K* (assumed to primarily represent bedrock properties since variables controlling hydrology and channel geometry stay the same). We then compare the imposed *K* to back-calculated "effective" erodibility K_{eff} from models that include the complicating effects of (a) sediment cover (SPACE model) and (b) local erosion rate variations caused by the geometry of horizontal rock layers (both SPM and SPACE). We calculate effective erodibilities by rearranging equation 6 (for SPM runs) and equation 7 (for SPACE runs), as described below.

In addition to varying particle settling velocity, we also explore how variations in sediment erodibility influence channel steepness and erosion rates. For this suite of model runs, *V* is held constant at 3.0 m/yr. For all model runs, the soft rock erodibility is held constant at 1.0x10^{-5} $m^{-0.5}yr^{-1}$. Finally, K_{sed} is varied to reflect different ratios of sediment to soft rock erodibility (Table 2). We test scenarios where the sediment is ten times more erodible than the soft rock (K_{sed}= 1.0 x10^{-4}), twice as erodible as the soft rock (K_{sed}= 2.0x10^{-5}), ten percent more erodible than the soft rock (K_{sed}= 1.1x10^{-5}), and finally a case where sediment is tenfold *less* erodible than the soft rock (K_{sed}= 5.0x10^{-6}). In natural rivers, coarse sediment from more resistant lithologies has been shown to exert a strong control on channel steepness (Johnson et al., 2009; Thaler & Covington, 2016). The K_{sed}= 5.0x10^{-6} run could conceptually reflect a scenario where the hard rock layer produces highly resistant, difficult to transport sediment that dominates the sediment load over both hard and soft bedrock channel reaches downstream (for example, in the form of large blocks that are initially detached by plucking rather than abrasion). We also explore three different erodibility contrasts between the soft and hard rocks. We set the default K for the hard rock to 2x10^{-6}, equal to 1/5th the erodibility of the soft rock. Additionally, we test K_{hard} = 1/3 and 1/2 K_{soft}. These ratios are comparable to and spanning the range of those used by Forte et al. (2016), and Perne et al. (2017) who used K_{hard}= 1/2 K_{soft} and 0.833 K_{soft}. Using a similar parameter space for bedrock erodibility contrasts allows us to interpret our results in the context of these previous works. A summary of the parameter space explored on the 50x50 cell model grids is presented in Table 2.

In layered landscapes, different rock types are exposed on the surface at different times and the landscape cannot achieve a true steady state where local vertically-measured incision rates remain constant (Perne et al., 2017). Nonetheless, averaged over the whole landscape area,

all models considered in our analysis approximate the dynamic steady-state condition of an essentially constant average elevation within their runtime.

3. Results

We first broadly compare two cases, a SPACE case and an SPM case, using a 200x200 cell model grid (Figure 2). We then systematically vary three main parameters in a series of model runs on smaller 50x50 cell grids: particle settling velocity (V), sediment erodibility (K_{sed}), and the erodibility ratio between the soft and hard rocks. When sediment cover is introduced, the steady state relief, or difference between maximum and minimum elevation of the entire landscape, increases by over forty percent (Figure 2). As the landscape is uplifted and the channels incise, the contacts between layers propagate upstream (Figure 3).

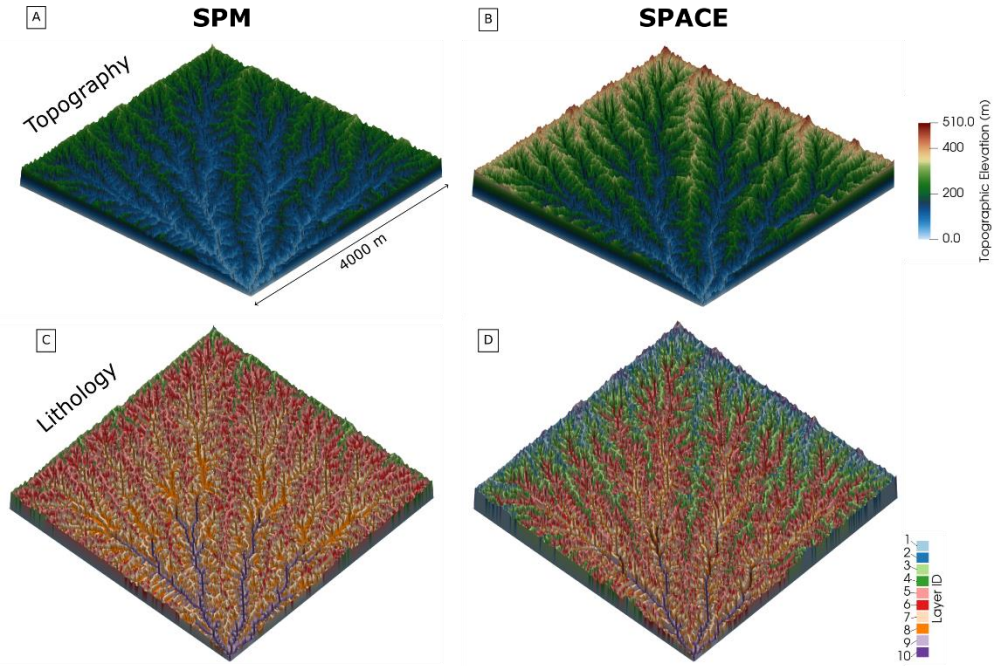

Figure 2. Three-dimensional view of dynamic steady state topography (A, B) and lithology (C, D) after 800 kyr of landscape evolution on 200x200 cell model grids. Both model runs have a constant and uniform uplift rate of 1.0 mm/yr. The SPM run with no sediment cover (A, C) has a lower overall steady state elevation compared to the SPACE model run (B, D).

In the SPACE run, more layers of rock are preserved and exposed in the landscape compared to the SPM run (Figure 2). The main channel in the SPM model run has a total relief of approximately 275 meters (Figure 3b) at the end of the 800 kyr runtime. Layers 1-3 have been completely eroded, and the majority of channel length is underlain by soft rock (layers 8 and 10). The SPACE model run has an additional 120 meters of relief along the main channel profile

(Figure 3d). In the SPACE model, sediment cover preferentially accumulates over the soft rock, where slopes are shallower and sediment entrainment rate is therefore lower (Equation 3).

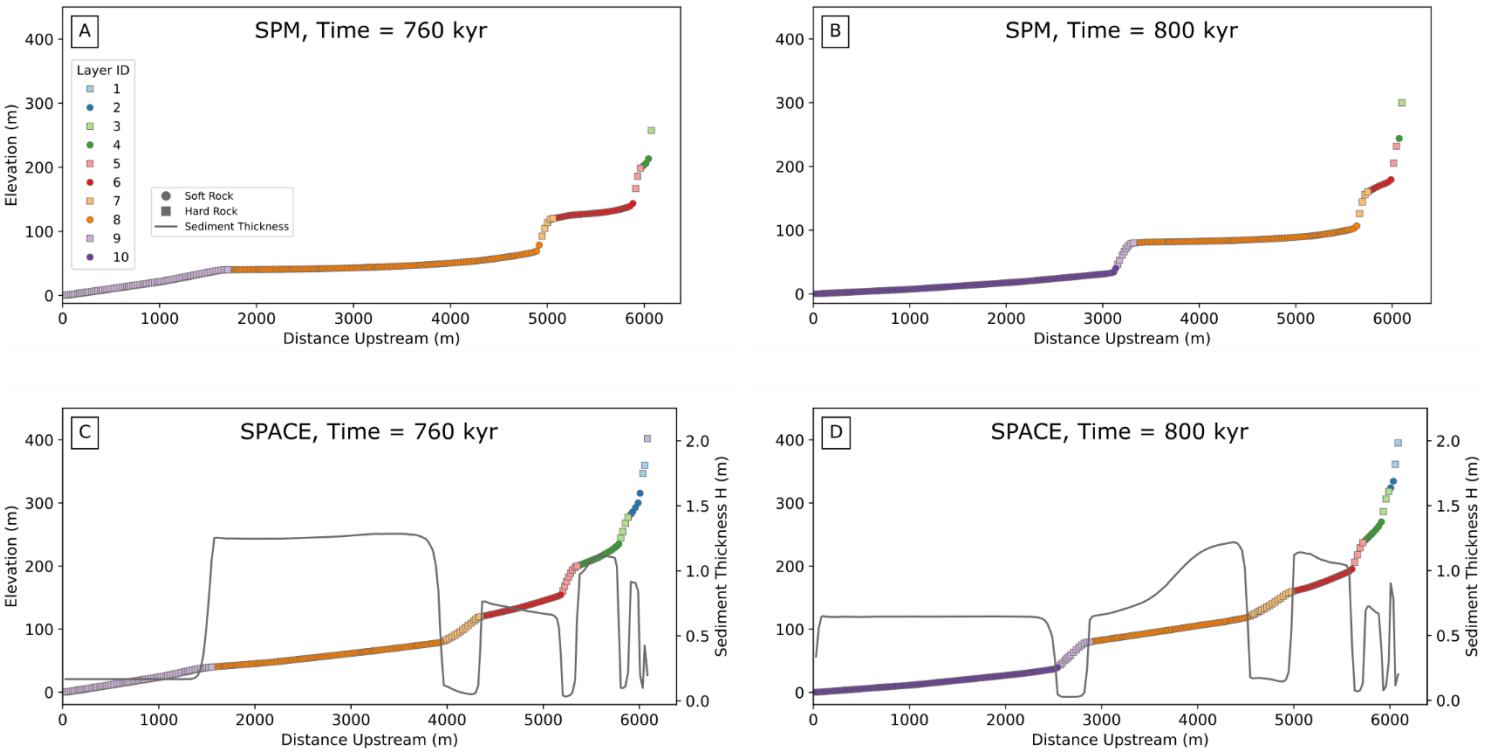

Figure 3. Main channel profiles for the SPM (A, B) and SPACE (C, D) simulations in Table 1 at two different time steps. These channels are also shown in map view in Figure 2. Each point along the channel profile represents the elevation at a node on the model grid. At the 760 kyr timestep (A, C), the downstream reach of the channel is underlain by hard rock. At the 800 kyr timestep (B, D), the contacts between layers have migrated upstream and the downstream reach is now underlain by soft rock. In the SPACE model run, sediment preferentially accumulates over reaches of soft rock.

3.1 Varying Particle Settling Velocity

In the SPACE model, the competition between rock uplift and sediment deposition is controlled by the dimensionless parameter *U/V*, which the authors refer to as the normalized rock uplift rate (Shobe et al. 2017). To explore how changing the relative rate of sediment deposition influences steady-state topography, we compare one SPM model run against three SPACE model runs with particle settling velocity, *V*, set to 1.0, 3.0, and 5.0 m/yr. The uplift rate is held constant at 1.0 mm/yr to yield dimensionless normalized uplift rates of .001, .003, and .005 m/yr. The contrast between the SPM and SPACE model runs illustrates how strongly sediment influences channel steepness (Figure 4). Compared to the SPM run, the SPACE runs have consistently steeper slopes in soft rocks and shallower slopes in hard rocks. We also compare channel steepness in

the model outputs to the steady-state steepness predictions for the hard and soft layers using equations 6 (for SPM) and 7 (for SPACE).

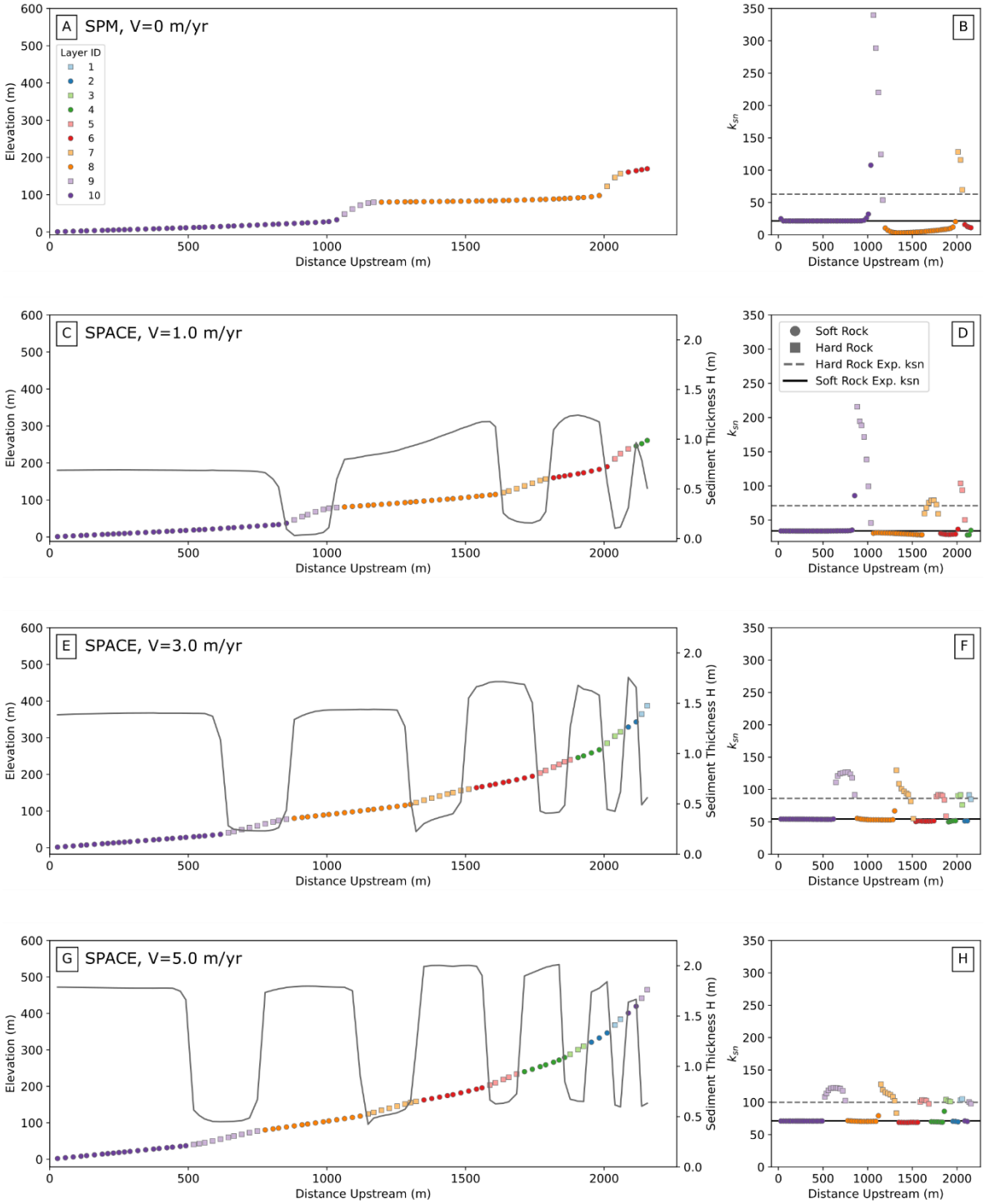

Figure 4. Main channel profiles (left) and normalized channel steepness k_{sn} (right) for four different model runs: one SPM (A, B) and three SPACE model runs with increasing particle settling velocity (B-H). Higher settling velocities correspond to coarser sediment and increased sediment cover in the channel. For the SPM case, particle settling velocity is effectively zero. Panel B uses equation (6) to calculate expected k_{sn}, while D, F, and H use equation (7).

3.1.1 Channel Steepness and Erosion Rates

For the SPM case with an imposed uplift rate of 1.0 mm/yr, the expected steady-state channel steepness (Equation 6) is 21.5 m for the soft rock and 63 m for the hard rock (Table 3). In the reach of soft rock immediately upstream of the outlet k_{sn} closely matches the expected value, then increases sharply in the nodes closest to the upstream contact with the hard rock layer (Figure 4). In the hard rock reaches, k_{sn} greatly exceeds the predicted value, and also varies more within a single reach than in the soft rock layers. In the downstream reach of hard rock, which shows the most extreme steepness variations, the maximum steepness index is roughly six times larger than the predicted value. In the SPM case, steepness in the soft rock is also substantially lower than predicted in the upstream reaches.

The SPACE model predicts that increasing sediment cover will increase channel steepness (Equation 7), and indeed we observe this in our SPACE runs (Figure 4). Across all three runs, k_{sn} in the soft rock layers generally matches the predicted values. As in the SPM case, k_{sn} in the hard rock is, on average, higher than expected for the SPACE model runs. In the V=1.0 m/yr model run, we again see a large increase in steepness in the downstream reach of hard rock. However, the amplitude of this increase is smaller relative to the SPM run due to the addition of sediment cover. As particle settling velocity increases to V=3.0 and V=5.0, the average steepness in the hard rock reaches begins to approach predicted SPACE values (Figure 4; Table 3). Additionally, k_{sn} within individual reaches of hard rock becomes more uniform as sediment cover increases.

Across all SPACE model runs, sediment cover preferentially accumulates over reaches of soft rock, which have shallower slopes. Sediment thickness is higher over lower slope sections because particle settling velocity, V, remains constant while sediment entrainment, E_s, is reduced over shallower slopes (Equation 3). In our model runs, lower slope reaches also correspond to lower erodibilities because the exponent n is set to 1.5 (i.e., n>1). The SPACE model predicts a uniform sediment thickness at steady state for a given bedrock and sediment erodibility. In the V1 model run, H is mostly uniform over the downstream reach of soft rock and over the hard rock reaches, but varies over the upstream layers of soft rock, where steepness is lower than predicted. As particle settling velocity increases to 3.0 then 5.0, H increases (equation 4) and generally becomes more uniform across individual lithologic reaches.

Variations in channel steepness and alluvial cover are closely tied to variations in local erosion rates (Figures 4, 5). Bedrock erosion rates along the channel profile vary as a function of underlying lithology, the thickness of sediment cover, and distance from a lithologic contact. Erosion rates tend to be highest on the downstream end of contacts where soft rock underlies hard rock. For all model runs, the reach of soft rock immediately upstream of the outlet (Layer 10), bedrock incision rates have adjusted to equal the uplift rate of 1.0 mm/yr (Figure 5). The SPM model (Figure 5a) shows the greatest variability in erosion rates upstream of this first soft reach, with the first hard rock reach (layer 9) having erosion rates as high as ≈10 mm/yr. Upstream in the next reach of soft rock (layer 8), the erosion rate drops to nearly zero. Erosion rates increase again at the next reach of hard rock (layer 7), but the increase is much smaller and the maximum erosion rate over this reach is roughly 3.0 mm/year. The variations in the local erosion rate along the profile reflect variations in channel steepness (Figure 4), with high erosion rates corresponding to higher-than-expected channel steepness for the imposed uplift rate. In the upstream reach of soft rock where erosion rates are low, channel steepness is also lower than predicted.

Bedrock incision rates in V1 model run (Figure 5b), which has the least amount of sediment cover, follow a similar pattern to the SPM case. In the SPM run, the bedrock incision rate increases to nearly ten times the uplift rate over the downstream reach of hard rock, then decreases to nearly zero in the next upstream reach of soft rock. However, the introduction of sediment cover lowers the hard rock peak incision rate in the V1 model run compared to the SPM run. The V3 and V5 model runs follow a similar general trend in local erosion rates along the channel profile, but amplitude of erosion rate variability is further reduced as sediment thickness H increases. Unlike bedrock erosion rates, sediment entrainment rates are relatively uniform along the channel profile (Figure 5b-d). While there are minor variations near the contacts, in general the competing influences of underlying lithology, slope, and the thickness of the alluvial layer balance out to maintain a steady entrainment rate.

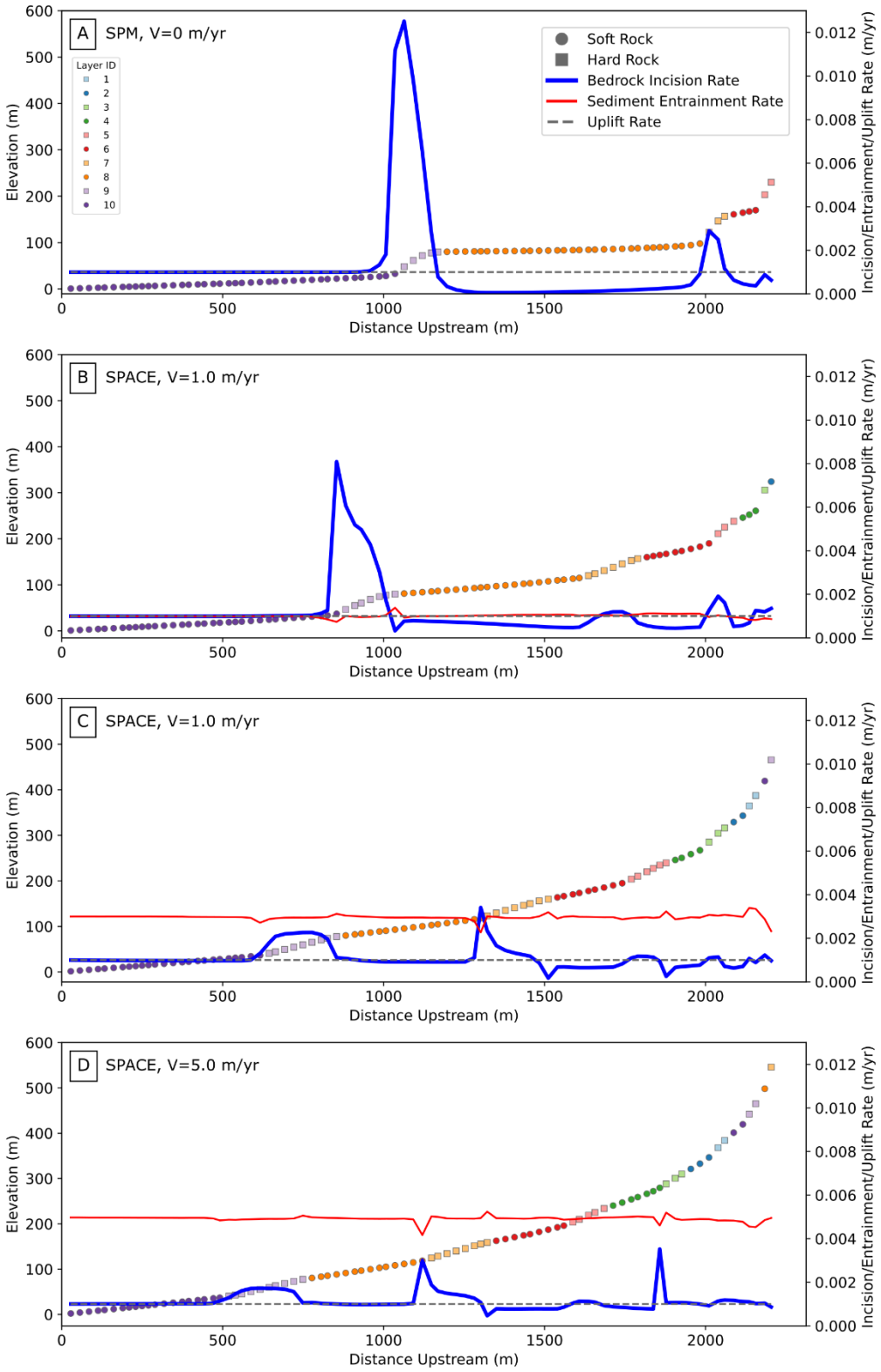

Figure 5. Local bedrock erosion rates along the main channel for one SPM model run (A) and SPACE model runs (B-D). The rock uplift rate of 1.0 mm/yr is shown in dashed lines. In the SPACE model runs (B-D), the sediment entrainment rate is shown in red. At true steady state, bedrock erosion rates along the channel profile should adjust to equal the uplift rate. However, changes in lithology result in variable erosion rates, particularly near the contacts between layers.

359

Our results illustrate feedbacks between bedrock incision, slope, and sediment cover that arise in layered rocks. Across all model runs, the local erosion rate in the downstream-most layer adjust to match the rate of relative base level fall (i.e., the rock uplift rate), and steepness similarly adjusts to match SPM and SPACE predictions. Upstream, feedbacks from variable lithology influence local erosion rates. For example, the layer 8 reach of soft rock has the same bedrock erodibility as the downstream reach (layer 10), but feedbacks from the contacts with hard rock layers both upstream and downstream result in significant steepness variations (Figure 4). Oversteepening (relative to steady-state steepness predictions) in hard rock layers is most pronounced in the SPM model run (Figure 4a), where vertically-measured erosion rates are highest (Figure 5a). As sediment cover is added to the system the impact of lithologic variability is reduced, resulting in smaller variations in both steepness (Figure 4b-h) and erosion rates (Figure 5b-d) and overall dampening the signal of the lithologic contact in the channel profile. In the SPACE model, the entrainment rate of sediment from the alluvial layer (Equation 3) is also dependent on slope, and as the slope of the underlying bedrock increases sediment thickness decreases. Erosion rates are influenced by both local reach slope and sediment thickness.

3.1.2 Effective Erodibility

The SPACE model runs have different dynamic steady state steepness values for the imposed uplift rate and erodibilities than predicted by the stream power model (Figure 4). This is important because the SPM is one of the most commonly used models for analyzing the topography of real river profiles. If a channel is at steady state and the uplift rate is known, the SPM (Equation 1) can be rearranged to $K = UA^{-m}S^{-n}$ to calculate erodibility using slope and drainage area, which are easily obtained from DEM data. When sufficient coarse sediment is present in the channel, the cover effect may make bedrock effectively less erodible than its imposed erodibility (K) values in the SPM model.

To understand how sediment cover may influence erodibility contrasts when applying the SPM framework to real landscapes, we calculate "effective erodibilities" of the rock layers from the steady-state model output in two ways (Figure 6). First, we assume that the *local* erosion rate E matches the landscape-averaged erosion rate $\bar{E}$, which in turn equals U (since the models are run until $\bar{E} = U = 1$ mm/yr). Applying regionally-determined erosion rates at local scales or locations different from where measured is a common implicit assumption in many quantitative

analyses (e.g. Cyr et al., 2014; DiBiase et al., 2010; Gasparini & Whipple, 2014; Snyder et al., 2000), as erosion rate data are usually drastically more limited than topographic data. For each lithologic reach along the main channel profile, we calculate the effective erodibility as $K_{eff} = UA^{-m}S^{-n}$, using the median reach drainage area and slope in order to minimize the influence of slope variability at contacts (Table 4; Figure 6a). Only the downstream reach of the SPM model run has an effective erodibility equal to the actual erodibility input into the model, because only in the most downstream reach is the local incision rate (measured vertically) equal to the uplift rate (Figure 5a). For the SPM model run (with no cover effect inhibiting incision and *V*=0), excluding the downstream reach, the soft rock is effectively *more* erodible than the imposed K_{soft} while the hard rock is effectively less erodible than K_{hard}.

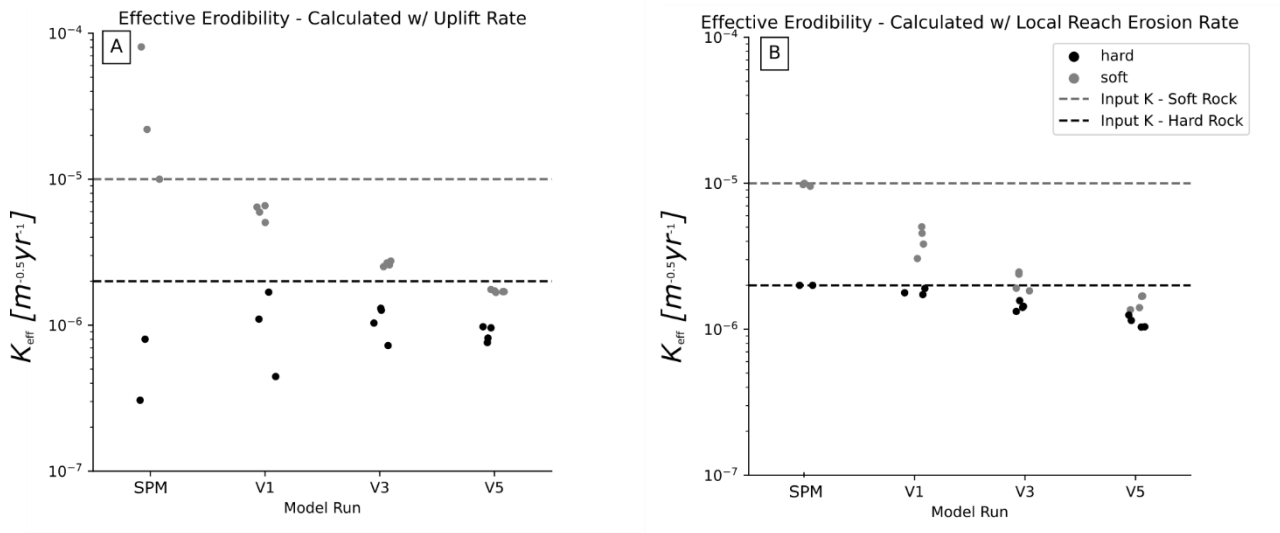

Figure 6. Effective erodibility calculated using the landscape-averaged erosion rate of 1.0 mm/yr (A) and the median local erosion rate for each lithologic reach along the channel (B) for four different model runs: An SPM run, which effectively has V=0, and three SPACE runs with particle settling velocity, V, set at 1.0, 3.0, and 5.0 mm/yr. Each data point represents the effective erodibility for an individual lithologic reach along the main channel for each model run. Variations in the x-axis positions of each point for a given model run are random and solely for the purpose of making data more visible.

In the SPACE model runs, effective erodibilities are lower than the model inputs for both rock types. As *V* increases and more sediment is deposited in the channel, effective erodibility decreases due to the cover effect. When no sediment is present (i.e. in the SPM run, which effectively has *V*=0), local erosion rates are most variable between contrasting layers (Figure 5). As sediment cover increases, the effective erodibility decreases as a result of the cover effect (Figure 6a). In the model run with the highest particle settling velocity, V5, the cover effect is so

powerful that the *effective* erodibility of the soft rock is lower than the *input* erodibility of the hard rock.

Second, we also calculate effective erodibilities using the median local erosion rate for each lithologic reach (rather than assuming $\bar{E} = U$) as $K_{eff} = EA^{-m}S^{-n}$ (equation 1). While the first method combines the effects of both sediment cover and spatial variation in erosion rate due to geometric effects of lithologic contrasts (Figure 6a), the second method is only sensitive to the sediment cover effects (Figure 6b). For the SPM model (again with no cover effect), the effective erodibilities for both rock types closely match the input erodibilities, as expected. For SPACE model runs, effective erodibilities for both hard and soft bedrock reaches systematically decrease as *V* increases, although the proportional decrease is much larger for the soft rock. The amount of decrease in each case simply represents the cover effect term e^{-H/H_*} in equation (2). For example, for the V5 model Figure 4d shows that the sediment thickness is ≈1.9 m over soft bedrock layers and ≈0.6 m over hard layers. Since $H_* = 1$, the proportional decrease in erodibility due to cover effects should be $e^{-H/H_*} \approx 0.15$ and ≈ 0.55 for soft and hard layers, respectively, which is quantitatively consistent with the V5 proportional decreases in effective erodibility in Figure 6b.

3.3 Sediment Erodibility

The thickness of the alluvial layer in the channel is fundamentally controlled by the balance between sediment deposition (controlled by *V*) and entrainment (controlled by discharge and sediment erodibility K_{sed}; Equation 3). As described above, the sediment entrainment ratio $K_{sed}q/V$ is one of several nondimensional parameters that control SPACE model behavior (Shobe et al., 2017). Using q = 1x10^6 m^3/yr as a reference unit discharge measured at 1 km^2 (the grid area for the 50x50 cell runs), Table 2 shows that model runs span a range of $K_{sed}q/V$ from 1.67 to 33.33. Like settling velocity, K_{sed} cannot be mapped directly to grain size in the SPACE model, but by exploring different ratios of K_{soft} to K_{sed}we illustrate how the contrast between the erodibility of rock and sediment alters the topographic expression of the different rock layers (Figure 7). Based the component of channel steepness controlled by sediment in the SPACE model at steady state (Equation 7), steepness should correlate positively with the ratio V/K_{sed}.

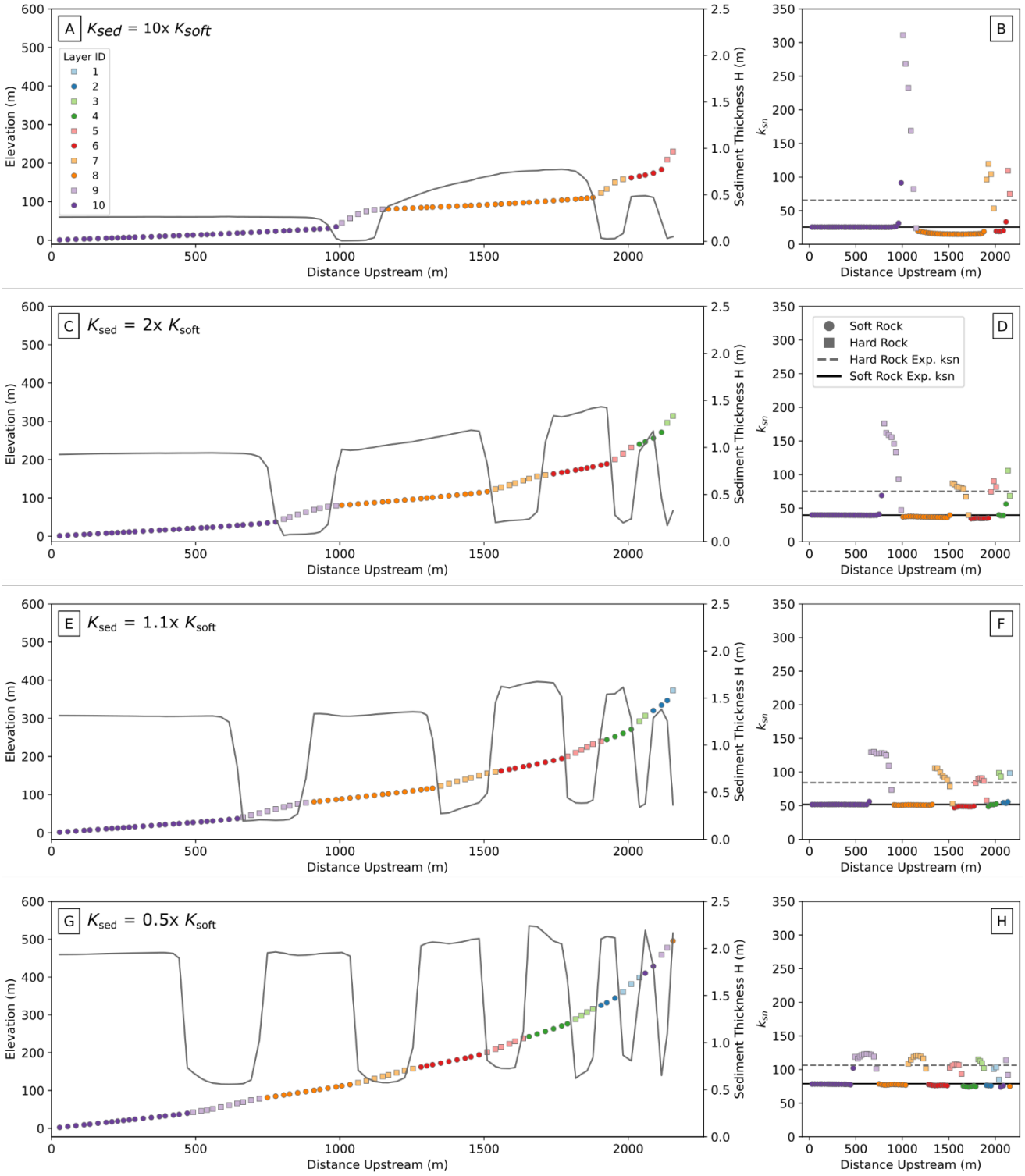

Figure 7. Channel profiles (left) and steepness (right) plots for four model runs with varying sediment erodibility (K_{sed}). K_{sed} increases from top to bottom (A), and with values to 1.0×10^{-4} (A, B), 2.0×10^{-5} (C, D), 1.1×10^{-5} (E, F), and 5.0×10^{-6} (G, H). The ratio of K_{sed}/V represents the competition between erosion and deposition. Decreasing values of K_{sed} reduce the steepness contrast between the two layers and simultaneously increases the average k_{sn} of each.

434

When $K_{sed}$is tenfold the erodibility of the soft rock, values of k_{sn} (Figure 7b) are generally similar to the output from the SPM model run and the sediment has little influence on channel steepness (Figure 4b). As the sediment erodibility is reduced, the lithologic contacts become less pronounced and we observe an overall increase in the both the predicted and actual steepness in soft rock reaches (Figure 7). Even though K_{hard} is held constant for these model runs, the predicted steepness in the hard rock reaches increases as K_{sed} is reduced (equation 7). Comparing figures 4 and 7, both sets of model runs demonstrate that as $K_{sed}q/V$ is decreased, the effect of sediment cover increases and the steepness contrast between the hard and soft lithologies is reduced. Figure 7 shows that reducing K_{sed} has the same influence on the channel as increasing particle settling velocity, increasing steepness in reaches of soft rock (as would be expected from Equation 7), but decreasing k_{sn} in hard rock (opposite what would be expected from equation 7). This is because the measured steepnesses are also influenced by the lithologic contrasts that affect local erosion rates due to geometric layer effects. In particular, Figure 5 shows that high vertically-measured erosion rates occur in the hard rock layers. These high erosion rates correspond to higher steepnesses in the hard rocks, with the vertical erosion rate contrast between hard and soft decreasing with increasing cover.

3.4 Bedrock Erodibility Contrasts

Unsurprisingly, steepness contrasts between hard and soft rock are primarily controlled by the erodibility contrast between the hard and the soft rocks (Figure 8). For model runs V3, KR3 and KR2 (Table 2), the erodibility of the soft rock is held constant at 1x10^{-5} $m^{-0.5}yr^{-1}$ while the erodibility of the hard rock is set to one-fifth, one-third, and one-half of the erodibility of the soft rock. The particle settling velocity is held constant at 3.0 m/yr. Less erodible hard layers result in steeper slopes and less sediment cover. In response to a twofold contrast in erodibility, there is a 17% increase in the average channel steepness from the soft to the hard rock. In contrast, for a fivefold contrast in K, which corresponds to an 80% reduction in erodibility, the hard rock is on average 80% steeper than the soft rock. The thickness of the alluvial layer over the soft rock stays relatively uniform across the three model runs, indicating that the thickness of alluvial cover is very sensitive to the underlying lithology and local slope, and less sensitive to upstream or downstream variations in steepness or erosion rate. There are minor increases in *H* upstream

of the first 1-2 soft layers of rock, but these variations are relatively small compared to the variations in the channel slope.

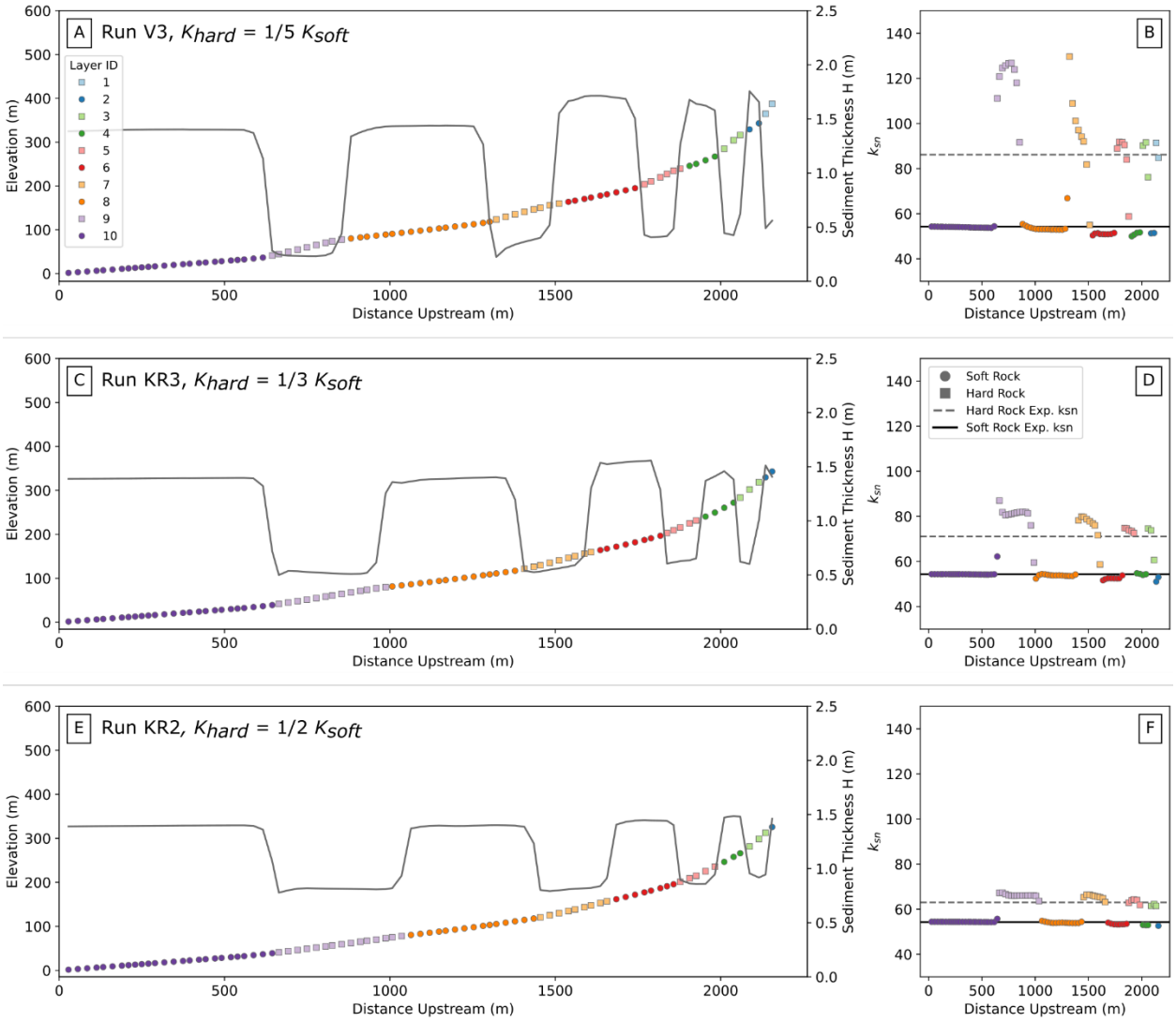

Figure 8. Three model runs with K_{hard} set to 1/5 (A, B), 1/3 (C, D) , and ½ (E, F) of K_{soft} . 1/5 is the default ratio used in other model runs. The soft rock erodibility is held constant at $1x10^{-5}$ while hard erodibilities correspond to $2x10^{-6}$ (A, B), $3.33x10^{-6}$ (C, D), and $5x10^{-6}$ (E, F). The profiles of the main channel for each model run are shown in the left column, and their corresponding channel steepness plots are shown in the right column. As the erodibility contrast between the soft and the hard rocks is reduced, the channel profile smooths out and the contrast in steepness between the two layers is reduced.

3.5 Landscape Adjustment Time

The degree of sediment cover also influences how long it takes the landscape to respond to the imposed rock uplift rate. At topographic steady state, spatially-averaged erosion rates adjust to match the rock uplift rate. While the local topography cannot reach true steady state because the

horizontal layering leads to spatial changes in bedrock erodibility through time (e.g., Perne and Covington, 2017), the landscape as a whole still adjusts to the imposed rock uplift rate by reaching a steady average elevation across the entire landscape (Figure 9a). In the SPM case, the landscape reaches a constant average elevation of approximately 110 meters after roughly 200 kyr. As more sediment cover is added to the system, the landscape takes longer to reach a steady average elevation, and the average elevation itself also increases. In the V5 model run (the case with the most sediment cover), the landscape has only just approached a constant average elevation of 275 meters by the end of the 1.2 myr model time. We also investigate whether the increased adjustment time is solely the result of the increased relief in the SPACE model outputs or a function of the sediment cover itself. To explore this question, we also included an additional SPM model run with the hard and soft layer erodibilities set to their respective average K_{eff} values calculated from the local erosion rates for the V5 model run, with K_{soft} = 1.56x10^{-6} and K_{hard} = 1.11x10^{-6} (see Figure 6b). The SPM-K_{eff} run using the effective erodibility values from the V5 run has a similar average elevation but reaches dynamic steady state in nearly half the time. The curve of sediment flux at the watershed outlet is also much smoother and adjusts more quickly, likely due to the relatively low contrast between K_{hard} and K_{soft} for this run (Figure 9b). That said, the absolute adjustment times presented above do not necessarily reflect the adjustment times of real landscapes. Instead, it is the relative differences in adjustment times between model runs that are meaningful.

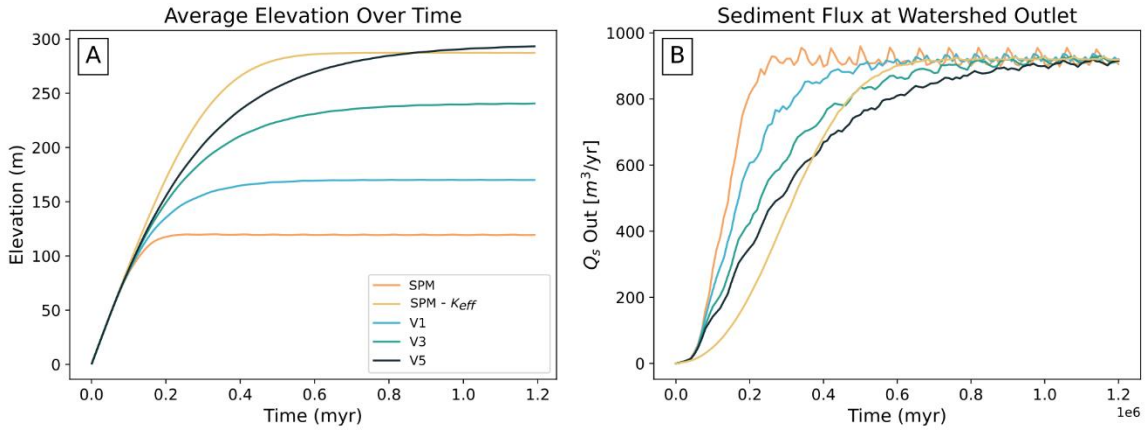

Figure 9. Landscape response to imposed uplift rate of 1.0 mm/yr for five model runs: two SPM runs and three SPACE runs with varying particle settling velocity. The SPM run uses the default erodibilities of 1x10^{-5} and 2x10^{-6} m$^{-0.5}$yr^{-1}. The SPM-K$_{eff}$ run uses the local effective erodibilities calculated for the V5 model run in order to produce a landscape with a comparable average elevation at steady state.

Similarly, the sediment flux at the watershed outlet varies as different layers are exposed, but for all model runs it reaches a steady average of approximately 922 m^3/yr, which is equal to the volume required to balance a rock uplift rate of 1.0 mm/yr across the 0.922 km^2 core grid area (which excludes boundary nodes)(Figure 9b). As the particle settling velocity increases, the sediment flux curve takes longer to flatten out. The cyclicity in flux out, most visible in the SPM model but present in all of the runs, has a period of 80 kyr. This reflects the time it takes to uplift two layers, a hard and soft pair, which in turn cause slope, sediment thickness, and therefore sediment flux variations near the outlet. For example, the transition from the layer at the outlet being soft bedrock (with a lower reach slope and thicker sediment) to hard bedrock leads to local steepening at the outlet, in turn decreasing the local thickness of sediment and causing a temporary increase in flux.

4. Discussion

The stream power model is widely used to interpret the topography of real landscapes and make inferences about lithology, climate, and tectonics (e.g., Baumann et al., 2018; Kirby & Whipple, 2001; Roberts & White, 2010; Seagren et al., 2020; Yanites et al., 2017; Zhong et al., 2022). While the SPM framework remains a powerful tool, our results demonstrate how strongly sediment cover effects may modulate erosion rates and patterns independent of bedrock erodibility. Our SPACE model runs show that in layered landscapes, sediment greatly diminishes the steepness contrast between different lithologies compared to the SPM model runs. The topographic expression of the contacts between rock layers is set by (a) the contrasting erodibilities between the different layers, and (b) the degree of sediment cover, which is controlled by the ratio of entrainment to deposition. Figure 10 conceptually illustrates feedbacks in layered rocks, both with and without cover effect feedbacks.

Local erosion rates change through time as a result of soft and hard layers being alternately exposed to the fixed rock uplift rate at the downstream end of the model domain (Figure 10a, 10c). Even as the overall landscape approximates equilibrium with spatially-averaged $E=U$, the erosional signal of the lithology at base level propagates up the channel, affecting local erosion rates. In eroding landscapes with non-vertical bedrock contacts, Perne and Covington (2017) demonstrated that true steady state topography (where the local erosion rate, measured vertically, is the same everywhere) cannot be attained because the erodibility of bedrock exposed at the surface changes in time and space. Instead, they quantified geometrically

how erosion adjusts towards a steady-state configuration of constant erosion measured parallel to contacts, which they termed erosional continuity. This is illustrated conceptually in Figure 10a, for parameter space qualitatively reminiscent of our SPM case (Figure 4a, 5a), at a particular time in which the downstream reach is a soft rock layer and the slope of that reach is adjusted to the base level lowering rate.

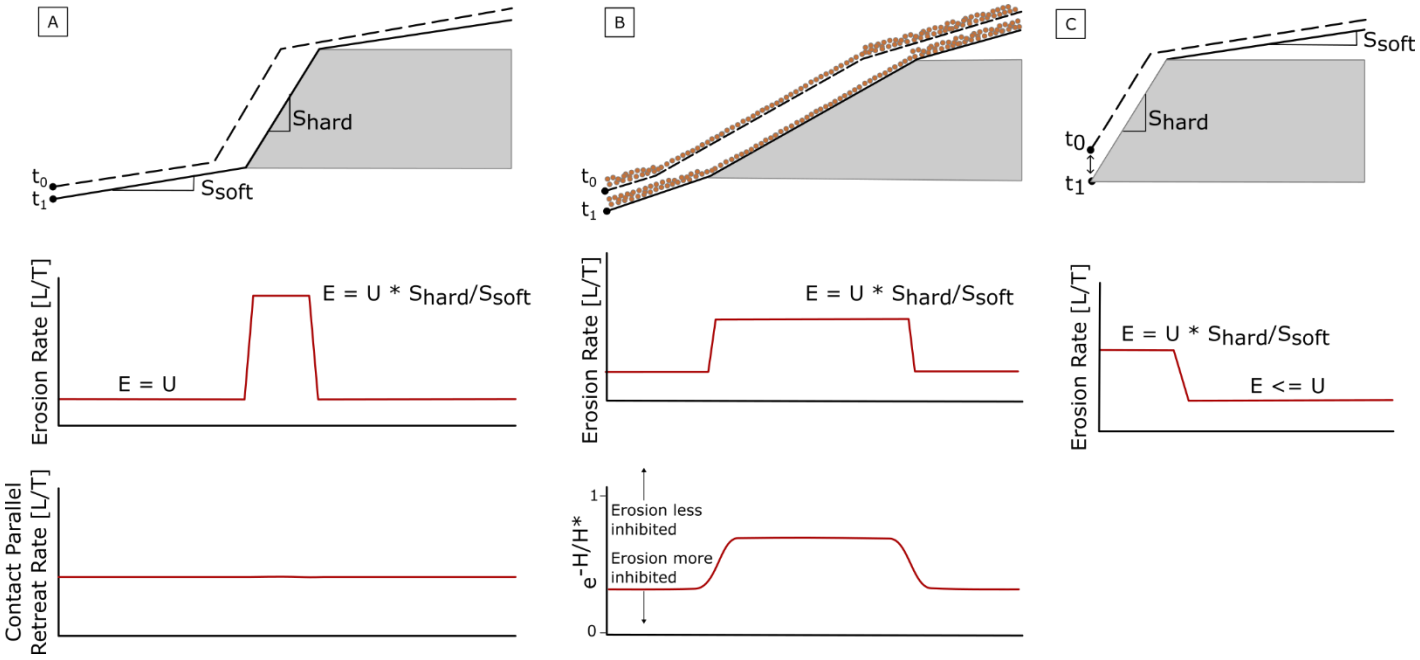

Figure 10. Conceptual figure illustrating the geometric feedbacks between layers with different erodibilities, and how sediment cover modulates those feedbacks. In all cases, erosion rate in the downstream reach adjusts to match the rate of base level fall. A and C illustrate a case with no sediment but different lithologic configurations, and B illustrates the dampening effects of sediment cover. When the lithology at the downstream reach is soft rock (A), erosion rates must increase in the overlying hard rock due to the undercutting of the soft rock. When sediment cover is present (B), the slope of the soft rock increases and the slope of the hard rock decreases compared to A, resulting in higher incision rates in the soft rock but lower rates in the hard rock. The strength of the cover effect is set by $e^{-H/H*}$where H is sediment thickness. Finally, when there is no sediment and soft rock overlies hard (C), erosion rates are higher downstream as the hard rock adjusts to erode at the rate of base level fall. When the soft rock overlies hard rock, the soft rock then erodes more slowly than U in order to maintain the same ratio of erosion rates.

Geometrically, rock uplift balanced by soft-rock incision ($E=U$) causes the position of the contact between soft and hard to migrate upstream. In both soft and hard layers, the horizontal retreat rate is U/S_{soft}, illustrating erosional continuity (Figure 10a). Simply because the hard rock channel slope is steeper ($S_{hard} > S_{soft}$, which occurs for n>1 provided that $K_{hard} < K_{soft}$), the local vertical base level lowering rate to which the hard rock layer responds is geometrically higher than U. Geometrically, if the soft layer is eroding at U, the hard layer adjusts to erode faster at $E = U \times S_{hard}/S_{soft}$. For example, our SPM model output (Figure 5a)

shows the first hard rock reach (layer 9) locally eroding at a rate up to 12 mm/yr. While this rate may seem anomalously high compared to U=1 mm/yr driving erosion, Forte et al. (2016) observed similarly large variations in erosion rates in their hard-over-soft rock model runs.

In comparison, Figure 10b conceptually illustrates how sediment cover modifies the fluvial topography of 10a, for parameter space qualitatively reminiscent of our V3 run (Figure 4e, 5c). The downstream soft bedrock layer is again adjusted to $E=U$, but sediment cover in the SPACE model reduces erosional efficiency—i.e., reduces the effective erodibility—by a factor of $e^{-H/H_*} = 0.22$ (for $H = 1.5$ m, $H_* = 1$ m) over the soft rock. Therefore, to incise at U, the soft rock channel reach steepens. Sediment also mantles the hard rock, but because the reach is steeper the sediment entrainment rate is higher (equation 3) and the sediment layer is thinner at $H = 0.5$ m. This also reduces hard rock effective erodibility, but only by a factor of $e^{-H/H_*} = 0.61$. So why does the reduction in hard rock K_{eff} not also cause the hard rock reach slope to steepen, like it did in the soft rock? The explanation is local base level: the increase in soft rock slope reduces both the horizontal retreat rate (U/S_{soft}) and the effective base level lowering rate "felt" by the hard rock (Figure 10a, b). The reduction in effective hard rock base level lowering rate more than offsets the decrease in hard rock K_{eff}, resulting in a lower reach slope in the hard rock layer. This combination of geometric and cover factors explains the overall trend of channel steepness increasing in soft rock layers but decreasing in hard rock layers, as cover effects become more important (increasing V or decreasing K_{sed}), over the parameter space shown in figures 4 and 7.

Another trend to explain in the model results is that the largest variations in both steepness and erosion rate tends to occur between the first hard layer upstream of the outlet and the soft layer upstream of that. The variations are largest in the SPM case (Figure 4b, 5a), with both steepness and erosion rate going from high values in the downstream reach of hard (layer 9) rock to nearly zero in the soft layer just above (layer 8). This spatial variability is due to alternating weak and strong layers being exposed at the downstream end of the channel and responding to the fixed uplift rate. Figure 10c conceptually illustrates the same parameter space as Figure 10a, but at a different time when the downstream-most exposed layer is hard rock rather than soft. In Figure 10c, the relative base level lowering rate to which the hard rock reach morphology adjusts is downstream boundary condition U. In contrast, in Figure 10a the hard rock reach responded to the higher rate $U \times S_{hard}/S_{soft}$, due geometrically to the lower slope of the downstream soft

layer. Furthermore, at the time shown in Figure 10c the soft layer responds to a relative base level fall rate $E = U\,S_{soft}/S_{hard}$, lower than U. The geometric relationships between slope and erosion rate in settings where the downstream reach is adjusted to base level fall are also illustrated in Perne et al. (2017) and Darling et al. (2020). Wolpert and Forte (2021) present a detailed of exploration of how lithologic signals at base level propagate upstream as contacts migrate.

Figure 9 shows that all of the model runs we presented essentially reached a landscape-averaged steady state elevation in which the landscape-averaged erosion rate matches the rock uplift rate. Even though the vertical rock uplift rate remains constant in our models, as hard and soft layers cycle through being exposed at the downstream boundary the horizontal retreat rate at this boundary varies (Figure 10a, c). The amplitude of this boundary condition perturbation gets damped as it migrates upstream during profile evolution, by erosion in the SPM model and additionally by sediment erosion and deposition in the SPACE model. For the SPM case, Perne et al. (2017) explored how quickly these base level perturbations were damped out, and generally found that the erosional signal from the lithology at the downstream boundary generally decays "after a couple rock contacts are passed". The downstream portions of our models are clearly influenced by cyclic horizontal retreat rate forcing due to the constant rock uplift rate boundary condition, consistent with other studies in layered rocks (Darling et al., 2020; Forte et al., 2016; Perne et al., 2017; Wolpert & Forte, 2021). The effects of changing lithology at the model boundary are similar in our study, but the variability that they impart in steepness, erosion rates and effective erodibilities do not change our interpretations. Additional variations in local steepness, erosion rate, and sediment thickness are likely caused by numerical approximations at the relatively small number of nodes we used in our models to solve the SPACE equations in Landlab (Shobe et al., 2017).

Compared to the SPM runs, the hard rock layers in the SPACE model runs have lower local erosion rates and lower k_{sn} values. The average steepness for both rock types in the SPACE runs is also higher than predicted by the SPACE model itself due to the influence of layers (equation 7). However, as the sediment entrainment ratio was decreased, whether by increasing V (Figure 4) or by decreasing K_{sed}, (Figure 7) the actual steepness indices approached the predicted values as a result of the reduced influence of bedrock erodibility contrasts. As the sediment cover effect becomes stronger the topographic expression of the erodibility contrast between layers becomes

weaker, although it does not disappear completely over the range of parameter space explored in this study (Figure 8). The underlying erodibility contrast between the layers is also important for determining the strength of the erosional signal from layers compared to the dampening caused by the cover effect. When the erodibility contrast between layers is reduced to only a twofold difference between the hard and the soft rock and cover effects are also present, the steepness contrast between the two rocks is greatly reduced (Figure 8e, 8f). For the particular parameter space of Figure 6a, sediment cover decreased the soft rock effective erodibility by up to an order of magnitude compared to the SPM case.

While the SPACE model is a powerful tool for exploring the feedbacks between bedrock erosion and sediment cover because it explicitly includes sediment mass balance and the cover effect, most of its parameters cannot be explicitly measured in the field. For example, grain size is not a model parameter, and effective settling velocity V does not correspond to actual grain settling velocities. Even if V could somehow be calibrated to grain size, linking measurable sediment properties to K_{sed} poses further difficulty. As such it would be challenging to quantitively validate the SPACE model based on field-measurable channel, sediment or hydrologic properties. The same is true for SPM parameters. Nonetheless, interpretations of real landscapes and rivers will likely continue to use the SPM framework because it has fewer parameters than SPACE and can be calibrated to DEMs if erosion rates are known. For some SPM applications, empirically calibrated erodibilities may be sufficient, but bedrock properties may only be a minor control on these values due in part to sediment cover effects. Sediment grain size also plays an important role in influencing the degree of cover effect. Field studies in a range of settings have shown that coarse sediment and boulders in particular from resistant lithologies significantly impact channel steepness (e.g., Anderson et al., 2023; Johnson et al., 2009; Shobe et al., 2020; Thaler & Covington, 2016). For example, Anderson et al. (2023) found that the steepest channel reaches in their study area were those armored with boulders from thick, resistant limestone beds. Thaler and Covington (2016) similarly found that channel steepness in their study was correlated with boulder size and percent boulder coverage rather than underlying bedrock lithology. These studies are in agreement with our model results in the regard that sediment cover significantly decreased the effective erodibility of the underlying bedrock, although it is worth noting that in these studies there was more sediment cover over steeper channel segments rather than shallower ones. In addition to the influence of grain size, changing

sediment supply in landscapes, such as may occur due to climate variability over different timescales (e.g., Fuller et al., 2009; Leeder et al., 1998), would also potentially change bedrock erodibilities in the stream power modeling framework.

In real landscapes, erodibility is a notoriously challenging parameter to independently quantify in terms of measurable rock properties. Many modeling studies in layered rocks use erodibility contrasts on the order of two to fivefold differences between different rock units to produce realistic topographies (e.g. Forte et al., 2016; Perne et al., 2017; Yanites et al., 2017). These results are in contrast with laboratory work suggesting that erodibility should inversely scale with a rock's tensile strength squared, and that tensile strength estimates for different rock types span over two orders of magnitude, if the erosion mechanism is bedload abrasion (Sklar & Dietrich, 2001). This range of tensile strength measurements, which was based on laboratory experiments, predicts much larger erodibility contrasts between different rock types than what has been observed in the field by fitting erosion rates and topographic data to the SPM. For example, in a global analysis of SPM parameters calculated using ^{10}Be denudation rates, Harel et al. (2016) found reduced erodibility in tectonically active areas compared to inactive ones. While they describe this observation as counterintuitive, our results suggest that decreased erodibility could be explained by increased sediment cover due to higher erosion rates in tectonically active settings. Our results demonstrate that sediment cover can significantly dampen the topographic expression of an erodibility contrast between two rock units, and the effective erodibilities of two rock types may be much lower, or span a narrower range of values, than mechanistic or process-based analyses of erodibility of exposed bedrock surfaces would suggest (Figure 6).

The increase in landscape adjustment time as V is increased (Figure 9) highlights how sediment cover may decrease bedrock erosion rates and slow down a landscape's overall response to imposed boundary conditions. Our work also shows that cover effects may slow landscape-scale equilibration as relief increases, not just decays. These results are qualitatively consistent with previous modeling studies, which explored landscape response to an increase in rock uplift rate and found that when sediment dynamics were considered time to reach a new steady state increased (e.g., Gasparini et al., 2007; Whipple & Tucker, 2002). A field study of boulder concentration in the Mendocino triple junction by Shobe et al. (2020) also suggested that coarse sediment cover could slow landscape response to tectonic forcing. In decaying landscapes, Egholm et al. (2018) found that coarse sediment input from hillslopes played a key

role in preserving topography in tectonically inactive settings. Baldwin et al. (2003) similarly interpreted that cover and erosion thresholds influenced by coarse sediment could explain the persistence of post-orogenic topography. Other field-based studies have explored how resistant caprock units, which provide a supply of large, durable boulders, can preserve high topography (e.g., Chilton & Spotila, 2020; Thaler & Covington, 2016). It is worth noting that the SPACE model formulation, as currently implemented, conserves sediment mass and accounts for flux, but is incomplete as it is not calibrated to reflect accurate rates of downstream advection and dispersion of sediment from one node to the next during a given timestep (e.g., Czuba et al., 2017) . This likely means that absolute rates of landscape adjustment and the timescales of sediment transport through the SPACE network are not necessarily realistic for real landscapes.

A key limitation in the current implementation of the SPACE model is that the sediment-size related parameters (V, K_{sed}) remain spatially and temporally constant. While beneficial for model simplicity and interpreting results, the model therefore does not include effects of downstream fining, or different sediment sizes or strengths being sourced from different bedrock lithologies. In real landscapes, sediment produced from different lithologies likely influences local reaches differently. For example, a highly fractured but otherwise strong rock type may produce relatively immobile coarse grains, while a softer lithology such as shale may produce much finer sediment. A recent field study highlighted how more resistant carbonate units produce larger boulders than the less resistant sandstones in the Guadalupe Mountains of Texas and New Mexico (Anderson et al., 2023). These carbonate boulders in turn were responsible for increasing steepness in downstream reaches of sandstone. The effect of variable sediment sizes and erodibilities from different lithologies is not captured in the model, but could potentially offset the reduction in erodibility contrasts that we find in our study.

Another SPACE model limitation is that it does not include the "tools" effect of sediment, where sediment enhances abrasion by impacting the bed. In real systems, some of the protective effect of sediment cover could be counteracted by increased abrasion from the tools effect. Future studies could expand on this work by modifying SPACE to include the tool effect of sediment and re-evaluating the contrast between the effective and actual erodibilities. Additional work could also explore the role of dynamic channel width, which may reduce steepness contrasts as channels can also widen to accommodate increased sediment load (Lague,

2010; Yanites, 2018). Modeling a dynamic channel width may also be important for improving model estimates of adjustment time (Attal et al., 2011).

Quantifying the erodibility of different lithologies in the field remains an outstanding challenge in geomorphology (e.g., Chilton & Spotila, 2022; Moore et al., 2009; Shobe et al., 2020; Zondervan et al., 2020). Unlike bedrock erodibility, sediment properties are easier to quantify. Grain size distributions can be measured in the field through point counting methods, or using new techniques for analyzing UAS imagery and airborne lidar (Chardon et al., 2020; Pearson et al., 2017), and transport relationships are well established for particle mobility and transport. Moving beyond the SPACE model, the relative ease of measuring sediment properties should hypothetically make it possible to separate out the effect of sediment load and cover on effective erodibility, while quantifying relationships between measurable rock properties and bedrock erodibility remains more challenging.

5. Conclusion

Our results demonstrate that the cover effect influences the topographic expression of lithologic contacts and can reduce the apparent erodibility of a given lithology. Over a range of parameter space, we test how relative differences in the amount of sediment cover and the erodibility contrasts between different rock layers compete to determine local erosion rates and channel steepness. In the Stream Power Model, which ignores sediment cover effects, reach slope and local erosion rate contrasts between weaker and stronger layers are large. As the amount of sediment cover increases, these variations are reduced and local erosion rates approach the landscape averaged erosion rate of 1.0mm/yr, equivalent to the uplift rate. Local erosion rates in turn influence channel steepness, which is a commonly used metric to interpret the topography of real landscapes. Our results demonstrate that a wide range of channel steepness indices can result from the same underlying erodibility configuration depending on the degree of sediment cover. When interpreting real landscapes assuming topographic equilibrium and applying the stream power model, it is important to consider the impact of sediment cover in reducing the apparent erodibilities of different rock units. This effect is particularly significant in layered landscapes, where sediment and lithologic feedbacks can have opposing influences on channel steepness.

Acknowledgements

The authors thank the Community Surface Dynamics Modeling System (CSDMS) for the training opportunities and coding assistance provided to G. Guryan and for developing and maintaining the Landlab toolkit. This research was funded by the National Science Foundation award no. 1918351 (JPLJ) and 1918459 (NMG).

Data Availability Statement

All code used to run the models and generate figures is currently available at https://github.com/gguryan and will be made available in a permanent repository. No additional data were used to create this manuscript.

Table 1. Model parameters for runs on 200x200 grids. Unless otherwise noted (e.g. in Table 2), SPACE parameters given here were also the default values used for the runs exploring parameter space on the 50x50 cell model grids.

Parameter	Parameter Description	SPM	SPACE
nx	# of x nodes	200	200
ny	# of y nodes	200	200
Node spacing (m)	-	20	20
Time step dt (yr)	-	40	40
Run time (kyr)	-	800	800
Rock layer thickness (m)	-	40	40
Uplift Rate (m/yr)	-	0.001	0.001
m (-)	Drainage area exponent	0.75	0.75
n (-)	Slope exponent	1.5	1.5
K_{soft} $(m^{-0.5}yr^{-1})$	Soft rock erodibility	$1.0x10^{-5}$	$1.0x10^{-5}$
K_{hard} $(m^{-0.5}yr^{-1})$	Hard rock erodibility	$2.0x10^{-6}$	$2.0x10^{-6}$
Hard/Soft ratio (-)	K_{hard}/K_{soft}	1/5	1/5
K_{sed} $(m^{-0.5}yr^{-1})$	Sediment erodibility	n/a	$1.1x10^{-5}$
V (m/yr)	Particle settling velocity	effectively 0	1.0
ω_{cr} (m/yr)	Bedrock erosion threshold	n/a	0
ω_{cs} (m/yr)	Sed. entrainment threshold	n/a	0
Initial sediment thickness (m)	-	n/a	0
H_* (m)	Sed. entrainment length scale	n/a	1
Φ (-)	Sediment porosity	n/a	0
Ff (-)	Fraction of fines (wash load)	n/a	0

Table 2. Summary of parameter space explored for the SPACE model runs in this study. Each of these models is run on a 50x50 cell square grid for 1.2 million years. All other SPACE model parameters are held constant to the values in Table 1. Run V3 represents our "default" SPACE parameters; input parameters that are varied from V3 values are bolded. For the SPM model run presented for comparison, the fraction of fines (F_f) parameter is set to 1.0 to force detachment-limited behavior. The dimensionless sediment entrainment ratio is $K_{sed}q/V$, and the bedrock erodibility ratio is K_{soft}/K_{hard} (Shobe et al., 2017). $K_{sed}q/V$ is calculated using 1x10^6 m^3/yr as a reference unit discharge measured at 1 km^2.

Parameter Varied	**Run ID**	**V** (m/yr)	K_{sed} $(m^{-0.5}yr^{-1})$	K_{hard} $(m^{-0.5}yr^{-1})$	$\frac{K_{sed}q}{V}$	$\frac{K_{sed}}{K_{soft}}$	$\frac{K_{soft}}{K_{hard}}$
Particle Settling Velocity	V1	**1.0**	1.0x10^{-5}	2.0x10^{-6}	10.00	1.0	5.0
	V3	3.0	1.0x10^{-5}	2.0x10^{-6}	3.33	1.0	5.0
	V5	**5.0**	1.0x10^{-5}	2.0x10^{-6}	2.00	1.0	5.0
Sediment Erodibility	Ksr 0.5	3.0	**5.0x10^{-6}**	2.0x10^{-6}	1.67	0.5	5.0
	Ksr 1.1	3.0	**1.1x10^{-6}**	2.0x10^{-6}	3.67	1.1	5.0
	Ksr 2.0	3.0	**2.0x10^{-5}**	2.0x10^{-6}	6.67	2.0	5.0
	Ksr 10	3.0	**1.0x10^{-4}**	2.0x10^{-6}	33.33	10.0	5.0
Bedrock Erodibility Ratio	Kr 2	3.0	1.0x10^{-5}	**5.0x10^{-6}**	3.33	1.0	**2.0**
	Kr 3	3.0	1.0x10^{-5}	**3.33x10^{-6}**	3.33	1.0	**3.0**
SPM Default	SPM	0	n/a	2.0x10^{-6}	n/a	n/a	5.0
SPM - K_{eff}	SPMK	0	n/a	1.56x10^{-6}	n/a	n/a	1.4

Table 3. Actual vs. Expected Normalized Channel Steepness (k_{sn}) for 50x50 cell grids comparing the detachment-limited case to three iterations of the SPACE model with particle settling velocity varied from 1.0 to 5.0 m/yr. The expected steepness is calculated assuming that the landscape-averaged erosion rate, E, is equal to the uplift rate, U, of 1.0 mm/yr. Equation 6 is used to calculate expected steepness for the SPM case and Equation 7 is used for the SPACE runs.

Rock Type	**Layer ID**	**SPM**	**V1**	**V3**	**V5**
Soft	10	24.1	35.6	54.0	70.9
Hard	9	205.4	150.6	118.8	117.0
Soft	8	6.4	30.2	54.2	71.2
Hard	7	104.6	70.4	95.0	110.2
Soft	6	12.9	30.2	51.0	68.9
Hard	5	-	82.7	84.3	101.5
Soft	4	-	30.5	50.9	72.0
Hard	3	-	-	86.0	102.3
Soft	2	-	-	-	70.2
Hard	1	-	-	-	-
Soft Rock Average k_{sn}		**14.5**	**31.6**	**52.6**	**70.6**
Soft Rock Expected k_{sn}		21.5	34.2	54.3	71.1
Hard Rock Average k_{sn}		**155.0**	**101.2**	**96.0**	**107.7**
Hard Rock Expected k_{sn}		63	71.14	86.18	100

Table 4. Effective Erodibilities Calculated from the Stream Power Incision Model; erodibility units are $m^{-0.5}yr^{-1}$. These data correspond to Figure 6a. K_{eff} is calculated using the median slope and drainage area for each lithologic reach and assuming an erosion rate of 1.0 mm/year (equal to the uplift rate, E=U). The reach IDs are listed in descending order from downstream (10) to 1 (upstream) (Figure 1). Only reaches with 3 nodes or greater are included in this analysis.

Rock Type	Layer ID	SPM	V1	V3	V5
Soft	10	$9.99x10^{-6}$	$5.05x10^{-6}$	$2.52x10^{-6}$	$1.68x10^{-6}$
Hard	9	$3.06x10^{-7}$	$4.45x10^{-7}$	$7.25x10^{-7}$	$7.60x10^{-7}$
Soft	8	$8.06x10^{-5}$	$5.95x10^{-6}$	$2.58x10^{-6}$	$1.70x10^{-6}$
Hard	7	$8.01x10^{-7}$	$1.68x10^{-6}$	$1.03x10^{-6}$	$8.16x10^{-7}$
Soft	6	$2.19x10^{-5}$	$6.44x10^{-6}$	$2.75x10^{-6}$	$1.76x10^{-6}$
Hard	5	-	$1.10x10^{-6}$	$1.27x10^{-6}$	$9.59x10^{-7}$
Soft	4	-	$6.59x10^{-6}$	$2.67x10^{-6}$	$1.72x10^{-6}$
Hard	3	-	-	$1.30x10^{-6}$	$9.76x10^{-7}$
Soft	2	-	-	-	$1.70x10^{-6}$
Hard	1	-	-	-	-
Soft Avg. K_{eff}		$3.75x10^{-5}$	$6.01x10^{-6}$	$2.63x10^{-6}$	$1.71x10^{-6}$
Soft Input K		$1.00x10^{-5}$	$1.00x10^{-5}$	$1.00x10^{-5}$	$1.00x10^{-5}$
Hard Avg K_{eff}		$5.54x10^{-7}$	$1.08x10^{-6}$	$1.08x10^{-6}$	$8.78x10^{-7}$
Hard Input K		$2.00x10^{-6}$	$2.00x10^{-6}$	$2.00x10^{-6}$	$2.00x10^{-6}$

References

Anderson, S., Gasparini, N., & Johnson, J. (2023). Building a bimodal landscape: bedrock lithology and bed thickness controls on the morphology of Last Chance Canyon, New Mexico, USA. *Earth Surface Dynamics*, *11*(5), 995–1011. https://doi.org/10.5194/esurf-11-995-2023

Attal, M., Cowie, P. A., Whittaker, A. C., Hobley, D., Tucker, G. E., & Roberts, G. P. (2011). Testing fluvial erosion models using the transient response of bedrock rivers to tectonic forcing in the Apennines, Italy. *Journal of Geophysical Research: Earth Surface*, *116*(2), 2005. https://doi.org/10.1029/2010JF001875

Baldwin, J. A., Whipple, K. X., & Tucker, G. E. (2003). Implications of the shear stress river incision model for the timescale of postorogenic decay of topography. *Journal of Geophysical Research: Solid Earth*, *108*(B3). https://doi.org/10.1029/2001jb000550

Barnhart, K. R., Hutton, E., Gasparini, N., & Tucker, G. (2018). Lithology: A Landlab submodule for spatially variable rock properties. *Journal of Open Source Software*, *3*(30), 979. https://doi.org/10.21105/joss.00979

Barnhart, K. R., Tucker, G. E., Doty, S. G., Shobe, C. M., Glade, R. C., Rossi, M. W., & Hill, M. C. (2020). Inverting Topography for Landscape Evolution Model Process Representation: 3.

744 Determining Parameter Ranges for Select Mature Geomorphic Transport Laws and Connecting
745 Changes in Fluvial Erodibility to Changes in Climate. *Journal of Geophysical Research: Earth*
746 *Surface*, *125*(7), 1–34. https://doi.org/10.1029/2019JF005287

747 Baumann, S., Robl, J., Prasicek, G., Salcher, B., & Keil, M. (2018). The effects of lithology and base
748 level on topography in the northern alpine foreland. *Geomorphology*, *313*, 13–26.
749 https://doi.org/10.1016/j.geomorph.2018.04.006

750 Chardon, V., Schmitt, L., Piégay, H., & Lague, D. (2020). Use of terrestrial photosieving and airborne
751 topographic LiDAR to assess bed grain size in large rivers: a study on the Rhine River. *Earth*
752 *Surface Processes and Landforms*, *45*(10), 2314–2330. https://doi.org/10.1002/esp.4882

753 Chilton, K. D., & Spotila, J. A. (2020). Preservation of Valley and Ridge topography via delivery of
754 resistant, ridge-sourced boulders to hillslopes and channels, Southern Appalachian Mountains,
755 U.S.A. *Geomorphology*, *365*, 107263. https://doi.org/10.1016/j.geomorph.2020.107263

756 Chilton, K. D., & Spotila, J. A. (2022). Uncovering the Controls on Fluvial Bedrock Erodibility and
757 Knickpoint Expression: A High-Resolution Comparison of Bedrock Properties Between
758 Knickpoints and Non-Knickpoint Reaches. *Journal of Geophysical Research: Earth Surface*,
759 *127*(3). https://doi.org/10.1029/2021JF006511

760 Crosby, B. T., & Whipple, K. X. (2006). Knickpoint initiation and distribution within fluvial networks:
761 236 waterfalls in the Waipaoa River, North Island, New Zealand. *Geomorphology*, *82*(1–2), 16–38.
762 https://doi.org/10.1016/j.geomorph.2005.08.023

763 Cyr, A. J., Granger, D. E., Olivetti, V., & Molin, P. (2014). Distinguishing between tectonic and
764 lithologic controls on bedrock channel longitudinal profiles using cosmogenic 10Be erosion rates
765 and channel steepness index. *Geomorphology*, *209*, 27–38.
766 https://doi.org/10.1016/j.geomorph.2013.12.010

767 Czuba, J. A., Foufoula-Georgiou, E., Gran, K. B., Belmont, P., & Wilcock, P. R. (2017). Interplay
768 between spatially explicit sediment sourcing, hierarchical river-network structure, and in-channel
769 bed material sediment transport and storage dynamics. *Journal of Geophysical Research: Earth*
770 *Surface*, *122*(5), 1090–1120. https://doi.org/10.1002/2016JF003965

771 Darling, A., Whipple, K., Bierman, P., Clarke, B., & Heimsath, A. (2020). Resistant rock layers amplify
772 cosmogenically-determined erosion rates. *Earth Surface Processes and Landforms*, *45*(2), 312–330.
773 https://doi.org/10.1002/ESP.4730

774 Davy, P., & Lague, D. (2009). Fluvial erosion/transport equation of landscape evolution models revisited.
775 *J. Geophys. Res*, *114*, 3007. https://doi.org/10.1029/2008JF001146

776 DiBiase, R. A., Whipple, K. X., Heimsath, A. M., & Ouimet, W. B. (2010). Landscape form and
777 millennial erosion rates in the San Gabriel Mountains, CA. *Earth and Planetary Science Letters*,
778 *289*(1–2), 134–144. https://doi.org/10.1016/j.epsl.2009.10.036

779 DiBiase, R. A., Denn, A. R., Bierman, P. R., Kirby, E., West, N., & Hidy, A. J. (2018). Stratigraphic
780 control of landscape response to base-level fall, Young Womans Creek, Pennsylvania, USA. *Earth*
781 *and Planetary Science Letters*, *504*, 163–173. https://doi.org/10.1016/j.epsl.2018.10.005

782 Egholm, D. L., Knudsen, M. F., & Sandiford, M. (2013). Lifespan of mountain ranges scaled by
783 feedbacks between landsliding and erosion by rivers. *Nature*, *498*(7455), 475–478.
784 https://doi.org/10.1038/nature12218

785 Ferrier, K. L., Huppert, K. L., & Perron, J. T. (2013). Climatic control of bedrock river incision. *Nature*,
786 *496*(7444), 206–209. https://doi.org/10.1038/nature11982

787 Flint, J. J. (1974). Stream gradient as a function of order, magnitude, and discharge. *Water Resources*
788 *Research*, *10*(5), 969–973. https://doi.org/10.1029/WR010i005p00969

789 Forte, A. M., Yanites, B. J., & Whipple, K. X. (2016). Complexities of landscape evolution during
790 incision through layered stratigraphy with contrasts in rock strength. *Earth Surface Processes and*
791 *Landforms*, *41*(12), 1736–1757. https://doi.org/10.1002/esp.3947

792 Fuller, T. K., Perg, L. A., Willenbring, J. K., & Lepper, K. (2009). Field evidence for climate-driven
793 changes in sediment supply leading to strath terrace formation. *Geology*, *37*(5), 467–470.
794 https://doi.org/10.1130/G25487A.1

795 Gasparini, N. M., & Whipple, K. X. (2014). Diagnosing climatic and tectonic controls on topography:
796 Eastern flank of the northern Bolivian Andes. *Lithosphere*, *6*(4), 230–250.
797 https://doi.org/10.1130/L322.1

798 Gasparini, N. M., Whipple, K. X., & Bras, R. L. (2007). Predictions of steady state and transient
799 landscape morphology using sediment-flux-dependent river incision models. *Journal of Geophysical*
800 *Research: Earth Surface*, *112*(3), 1–20. https://doi.org/10.1029/2006JF000567

801 Hancock, G. S., & Anderson, R. S. (2002). Numerical modeling of fluvial strath-terrace formation in
802 response to oscillating climate. *GSA Bulletin*, *11*(9), 1131–1142. Retrieved from
803 http://pubs.geoscienceworld.org/gsa/gsabulletin/article-pdf/114/9/1131/3388895/i0016-7606-114-9-

1131.pdf

Harel, M.-A., Mudd, S. M., & Attal, M. (2016). Global analysis of the stream power law parameters based on worldwide 10 Be denudation rates. https://doi.org/10.1016/j.geomorph.2016.05.035

Hobley, D. E. J., Adams, J. M., Siddhartha Nudurupati, S., Hutton, E. W. H., Gasparini, N. M., Istanbulluoglu, E., & Tucker, G. E. (2017). Creative computing with Landlab: An open-source toolkit for building, coupling, and exploring two-dimensional numerical models of Earth-surface dynamics. *Earth Surface Dynamics*, *5*(1), 21–46. https://doi.org/10.5194/esurf-5-21-2017

Howard, A. D., & Kerby, G. (1983). Channel changes in badlands. *Geological Society of America Bulletin*, *94*(6), 739–752. https://doi.org/10.1130/0016-7606(1983)94<739:CCIB>2.0.CO;2

Howard, Alan D. (1994). A detachment-limited model of drainage basin evolution. *Water Resources Research*, *30*(7), 2261–2285. https://doi.org/10.1029/94WR00757

Johnson, J. P. L. L., Whipple, K. X., Sklar, L. S., & Hanks, T. C. (2009). Transport slopes, sediment cover, and bedrock channel incision in the Henry Mountains, Utah. *Journal of Geophysical Research*, *114*(2), F02014. https://doi.org/10.1029/2007JF000862

Kirby, E., & Whipple, K. (2001). Quantifying differential rock-uplift rates via stream profile analysis. *Geology*, *29*(5), 415–418. https://doi.org/10.1130/0091-7613(2001)029<0415:QDRURV>2.0.CO;2

Kirby, E., & Whipple, K. X. (2012). Expression of active tectonics in erosional landscapes. *Journal of Structural Geology*, *44*, 54–75. https://doi.org/10.1016/j.jsg.2012.07.009

Lague, D. (2010). Reduction of long-term bedrock incision efficiency by short-term alluvial cover intermittency. *Journal of Geophysical Research: Earth Surface*, *115*(F2). https://doi.org/10.1029/2008jf001210

Lague, D. (2014). The stream power river incision model: Evidence, theory and beyond. *Earth Surface Processes and Landforms*, *39*(1), 38–61. https://doi.org/10.1002/esp.3462

Leeder, M. R., Harris, T., & Kirkby, M. J. (1998). Sediment supply and climate change: implications for basin stratigraphy. *Basin Research*, *10*(1), 7–18. https://doi.org/10.1046/j.1365-2117.1998.00054.x

Moore, J. R., Sanders, J. W., Dietrich, W. E., & Glaser, S. D. (2009). Influence of rock mass strength on the erosion rate of alpine cliffs. *Earth Surface Processes and Landforms*, *34*(10), 1339–1352. https://doi.org/10.1002/esp.1821

Müller-Hagmann, M., Albayrak, I., Auel, C., & Boes, R. M. (2020). Field investigation on hydroabrasion

in high-speed sediment-laden flows at sediment bypass tunnels. *Water (Switzerland)*, *12*(2), 10–16. https://doi.org/10.3390/w12020469

Murphy, B. P., Johnson, J. P. L., Gasparini, N. M., & Sklar, L. S. (2016). Chemical weathering as a mechanism for the climatic control of bedrock river incision. *Nature*. https://doi.org/10.1038/nature17449

Neely, A. B., & DiBiase, R. A. (2020). Drainage Area, Bedrock Fracture Spacing, and Weathering Controls on Landscape-Scale Patterns in Surface Sediment Grain Size. *Journal of Geophysical Research: Earth Surface*, *125*(10), 1–22. https://doi.org/10.1029/2020JF005560

Norton, K., & Schlunegger, F. (2011). Migrating deformation in the Central Andes from enhanced orographic rainfall. *Nature Communications*, *2*(1). https://doi.org/10.1038/ncomms1590

Pavano, F., Pazzaglia, F. J., & Catalano, S. (2016). Knickpoints as geomorphic markers of active tectonics: A case study from northeastern Sicily (southern Italy). *Lithosphere*, *8*(6), 633–648. https://doi.org/10.1130/L577.1

Pearson, E., Smith, M. W., Klaar, M. J., & Brown, L. E. (2017). Can high resolution 3D topographic surveys provide reliable grain size estimates in gravel bed rivers? *Geomorphology*, *293*(May), 143–155. https://doi.org/10.1016/j.geomorph.2017.05.015

Perne, M., Covington, M. D., Thaler, E. A., & Myre, J. M. (2017). Steady state, erosional continuity, and the topography of landscapes developed in layered rocks. *Earth Surface Dynamics*, *5*(1), 85–100. https://doi.org/10.5194/esurf-5-85-2017

Roberts, G. G., & White, N. (2010). Estimating uplift rate histories from river profiles using African examples. *Journal of Geophysical Research: Solid Earth*, *115*(2), 1–24. https://doi.org/10.1029/2009JB006692

Scott, D. N., & Wohl, E. E. (2019). Bedrock fracture influences on geomorphic process and form across process domains and scales. *Earth Surface Processes and Landforms*. https://doi.org/10.1002/esp.4473

Seagren, E. G., Schoenbohm, L. M., Owen, L. A., Figueiredo, P. M., Hammer, S. J., Rimando, J. M., et al. (2020). Lithology, topography, and spatial variability of vegetation moderate fluvial erosion in the south-central Andes. *Earth and Planetary Science Letters*, *551*. https://doi.org/10.1016/j.epsl.2020.116555

Shobe, C. M., Tucker, G. E., & Barnhart, K. R. (2017). The SPACE 1.0 model: A Landlab component for

2-D calculation of sediment transport, bedrock erosion, and landscape evolution. *Geoscientific Model Development*, *10*(12), 4577–4604. https://doi.org/10.5194/gmd-10-4577-2017

Shobe, C. M., Bennett, G. L., Tucker, G. E., Roback, K., Miller, S. R., & Roering, J. J. (2020). Boulders as a lithologic control on river and landscape response to tectonic forcing at the Mendocino triple junction. *Bulletin of the Geological Society of America*, *133*(3–4), 647–662. https://doi.org/10.1130/B35385.1

Sklar, L. S., & Dietrich, W. E. (2001). Sediment and rock strength controls on river incision into bedrock. *Geology*, *29*(12), 1087–1090. https://doi.org/10.1130/0091-7613(2001)029<1087:SARSCO>2.0.CO

Sklar, L. S., & Dietrich, W. E. (2004). A mechanistic model for river incision into bedrock by saltating bed load. *Water Resources Research*, *40*(6), 1–22. https://doi.org/10.1029/2003WR002496

Sklar, L. S., Riebe, C. S., Marshall, J. A., Genetti, J., Leclere, S., Lukens, C. L., & Merces, V. (2017). The problem of predicting the size distribution of sediment supplied by hillslopes to rivers. *Geomorphology*, *277*, 31–49. https://doi.org/10.1016/j.geomorph.2016.05.005

Snyder, N. P., Whipple, K. X., Tucker, G. E., & Merritts, D. J. (2000). Stream profiles in the Mendocino triple junction region, northern California. *GSA Bulletin*, *112*(8), 1250–1263.

Thaler, E. A., & Covington, M. D. (2016). The influence of sandstone caprock material on bedrock channel steepness within a tectonically passive setting: Buffalo National River Basin, Arkansas, USA. *Journal of Geophysical Research: Earth Surface*, *121*(9), 1635–1650. https://doi.org/10.1002/2015JF003771

Turowski, J. M., Lague, D., & Hovius, N. (2007). Cover effect in bedrock abrasion: A new derivation and its implications for the modeling of bedrock channel morphology. *Journal of Geophysical Research: Earth Surface*, *112*(4), 1–16. https://doi.org/10.1029/2006JF000697

Whipple, K. X., & Tucker, G. E. (1999). Dynamics of the stream-power river incision model: Implications for height limits of mountain ranges, landscape response timescales, and research needs. *Journal of Geophysical Research: Solid Earth*, *104*(B8), 17661–17674. https://doi.org/10.1029/1999jb900120

Whipple, K. X., & Tucker, G. E. (2002). Implications of sediment-flux-dependent river incision models for landscape evolution. *Journal of Geophysical Research*, *107*(B2). https://doi.org/10.1029/2000jb000044

Whittaker, A. C. (2012). How do landscapes record tectonics and climate? *Lithosphere*, *4*(2), 160–164.

https://doi.org/10.1130/RF.L003.1

Whittaker, A. C., Attal, M., Cowie, P. A., Tucker, G. E., & Roberts, G. (2008). Decoding temporal and spatial patterns of fault uplift using transient river long profiles. *Geomorphology*, *100*(3–4), 506–526. https://doi.org/10.1016/j.geomorph.2008.01.018

Wobus, C., Whipple, K. X., Kirby, E., Snyder, N., Johnson, J., Spyropolou, K., et al. (2006). Tectonics from topography: Procedures, promise, and pitfalls. *Special Paper of the Geological Society of America*, *398*, 55–74. https://doi.org/10.1130/2006.2398(04)

Wolpert, J. A., & Forte, A. M. (2021). Response of transient rock uplift and base level knickpoints to erosional efficiency contrasts in bedrock streams. *Earth Surface Processes and Landforms*, *46*(10), 2092–2109. https://doi.org/10.1002/ESP.5146

Yanites, B. J. (2018). The Dynamics of Channel Slope, Width, and Sediment in Actively Eroding Bedrock River Systems. *Journal of Geophysical Research: Earth Surface*, *123*(7), 1504–1527. https://doi.org/10.1029/2017JF004405

Yanites, B. J., Becker, J. K., Madritsch, H., Schnellmann, M., & Ehlers, T. A. (2017). Lithologic Effects on Landscape Response to Base Level Changes: A Modeling Study in the Context of the Eastern Jura Mountains, Switzerland. *Journal of Geophysical Research: Earth Surface*, *122*(11), 2196–2222. https://doi.org/10.1002/2016JF004101

Zhong, Y., Willett, S. D., Picotti, V., Xiong, J., & Zhang, H. (2022). Spatial and Temporal Variations of Incision Rate of the Middle Yellow River and Its Tributaries. *Journal of Geophysical Research: Earth Surface*, *127*(1). https://doi.org/10.1029/2021JF006327

Zondervan, J. R., Stokes, M., Boulton, S. J., Telfer, M. W., & Mather, A. E. (2020). Rock strength and structural controls on fluvial erodibility: Implications for drainage divide mobility in a collisional mountain belt. *Earth and Planetary Science Letters*, *538*, 116221. https://doi.org/10.1016/j.epsl.2020.116221